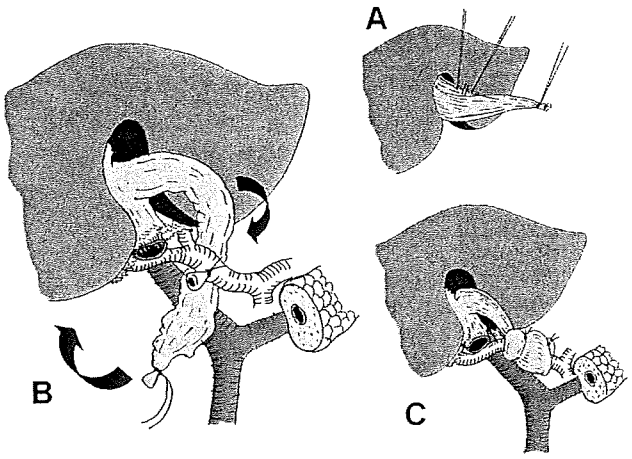

Figure 1. Schematic illustration of wrapping the stump of the gastroduodenal artery. (A) The fine vessels between the liver and the falciform ligament were ligated and divided and the ligament was extended as far as possible. (B) The common hepatic artery was wrapped using the falciform ligament to completely cover the stump of the gastroduodenal artery. Wrapping was performed counterclockwise to avoid concealing the orifice of the common bile duct. (C) The stump of the gastroduodenal artery was completely covered.

Figure 2. Wrapping the stump of the gastroduodenal artery. After the resection of the pancreatic head, the right hepatic artery (black arrow) was wrapped from the hepatic hilum to the root of the common hepatic artery (white arrow) using a customized falciform ligament. The stump of the distal pancreas was lifted upward using two stitches. The orifice of the common hepatic duct was clamped using forceps.

study group on pancreatic fistula,[8] that is, when the amylase concentration of the drained fluid obtained on or after postoperative day 3 was greater than 3 times the serum amylase concentration. Pancreatic fistulas were classified into grades A, B, and C according to severity; briefly, grade A was a "transient fistula," not associated with a delay in hospital discharge; a grade B fistula led to a delay in discharge, with a persistent drainage for more than 3 weeks; and a grade C fistula was usually associated with major complications.[8]

RESULTS

We successfully wrapped the stump of the GDA in all 136 patients who underwent pancreaticoduodenectomy; it took about 10 minutes to perform the wrapping. Postoperative CT examinations revealed an unenhanced low-density area, corresponding to the wrapped falciform ligament, surrounding the common hepatic artery (Fig. 3).

Postoperatively, 72 patients (53%) developed pancreatic fistulas; 22 patients had grade A fistulas, 40 had grade B fistulas, and 10 had grade C fistulas. Median amylase values of in-drain fluid collected on days 1 and 3 were 1,020 IU/L (range 1 to 26,000 IU/L) and 160 IU/L (range 7 to 15,000 IU/L), respectively. One patient developed significant hemorrhage associated with a pancreatic fistula; an 80-year-old man, who had undergone pylorus-preserving pancreaticoduodenectomy for treatment of ampullary cancer, developed intraabdominal bleeding from the stump of the GDA on day 18; the common hepatic artery was successfully embolized in this patient. Other complications included delayed gastric emptying in 37 patients (27%) and bile leakage in 4 patients (3%), and the overall morbidity rate was 67%. The median length of drain placement was 15 days and the median hospital stay was 27 days. No patients died from their operations.

DISCUSSION

The falciform ligament has been used during liver surgery to repair hepatic injuries, to prevent bile leakage from the dissected plane,[9,10] and to fix the right hemiliver and maintain adequate hepatic outflow.[11] But to our knowledge, use of this ligament to cover the stump of the GDA during pancreatic surgery has never been described. This technique is simple and easy to perform, and we believe that the procedure is useful for protecting the stump of the GDA from pancreatic juice and for preventing hemorrhages. Although 50 of our patients developed grade B or C pancreatic fistulas, only 1 patient experienced a hemorrhage from the stump of the GDA. Other authors have described the efficacy of an omental flap for covering the hepatic artery and portal vein during pancreaticoduodenectomies.[12,13] But such a

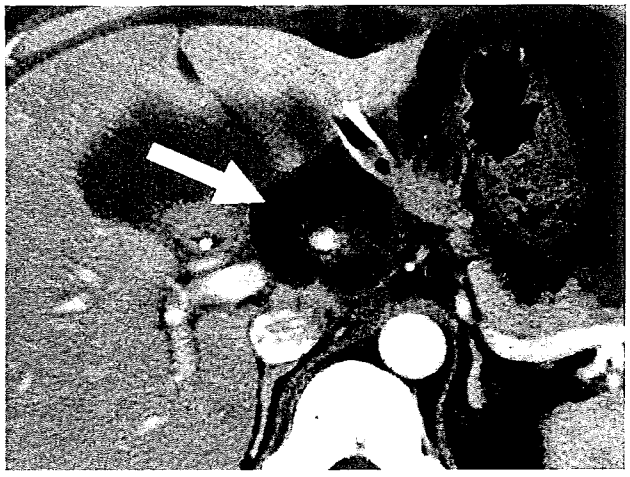

Figure 3. Postoperative CT scan showing the wrapped hepatic artery after a pancreaticoduodenectomy. The postoperative CT scan revealed a thick fat-density area, corresponding to the falciform ligament (white arrow), that completely wrapped a well-enhanced vessel, the hepatic artery. The drain was placed on the superior edge of the pancreaticojejunostomy.

flap necessitates division of the greater omentum and attention to ensure proper placement of the abundant adipose tissue.

The incidence of pancreatic fistulas at our institute is 53%, which is higher than that reported by other institutions. This relatively high incidence might be because of the definition of pancreatic fistula that is used; the international definition[8] includes minimal leakage of amylase-rich fluid on postoperative day 3 as a grade A pancreatic fistula; such leakage may have been neglected in other reports.[1-6]

Only one patient (2%) of the 50 patients with grade B or C fistulas developed a hemorrhage from the GDA on postoperative day 9. The reported incidence of massive hemorrhage in patients with pancreatic leakage is 16% to 40%.[5,6] So, hemorrhage may still occur even after the stump of the GDA has been wrapped, although the incidence of such hemorrhage in this study was lower than the reported incidence, and no mortalities occurred. This successful outcome might be from the advancement of surgical management, including the use of duct-to-duct pancreaticojejunostomies, adequate drainage of amylase-rich fluid, adequate usage of antibiotics, diagnostic accuracy as a result of CT scans, and interventional techniques. In addition, the simple wrapping technique that was used may have contributed to the prevention of bleeding. This method could also be used to cover the stump of the splenic artery during distal pancreatectomies.

In conclusion, we have introduced our simple and easy technique for wrapping the stump of the GDA using the falciform ligament. We believe that this method may contribute to the prevention of postoperative hemorrhages associated with pancreatic fistulas.

REFERENCES

1. Balcom JH IV, Rattner DW, Warshaw AL, et al. Ten-year experience with 733 pancreatic resections. Arch Surg 2001;136:391–398.
2. Adam U, Makowiec F, Riediger H, et al. Risk factors for complications after pancreatic head resection. Am J Surg 2004;187:201–208.
3. Kazanjian KK, Hines OJ, Eibl G, et al. Management of pancreatic fistulas after pancreaticoduodenectomy. Arch Surg 2005;140:849–855.
4. Muscari F, Suc B, Kirzin S, et al. Risk factors for mortality and intraabdominal complications after pancreatoduodenectomy: multivariate analysis in 300 patients. Surgery 2005;139:591–598.
5. Choi SH, Moon HJ, Heo JS, et al. Delayed hemorrhage after pancreaticoduodenectomy. J Am Coll Surg 2004;199:186–191.
6. Tien YW, Lee PH, Yang CY, et al. Risk factors of massive bleeding related to pancreatic leak after pancreaticoduodenectomy. J Am Coll Surg 2005;201:554–559.
7. Shimada K, Sakamoto Y, Sano T, Kosuge T. The role of paraaortic lymph node involvement on early recurrence and survival after macroscopic curative resection with extended lymphadenectomy for pancreatic carcinoma. J Am Coll Surg 2006;203:345–352.
8. Bassi C, Dervenis C, Butturini G, et al. Postoperative pancreatic fistula: an international study group (ISGPF) definition. Surgery 2005;138:8–13.
9. Fischer RP, Gervin AS. The use of falciform ligament in the repair of hepatic injuries. Surg Gynecol Obstet 1985;161:383–384.
10. Doerr RJ, Luchette FA, Gundlach ET, et al. Further clinical application of the falciform ligament. Surg Gynecol Obstet 1990;170:167–168.
11. Ogata S, Kianmanesh R, Belghiti J. Doppler assessment after right hepatectomy confirms the need to fix the remnant liver in the anatomical position. Br J Surg 2005;92:592–595.
12. Maeda A, Ebata T, Kanemoto H, et al. Omental flap in pancreaticoduodenectomy for protection of splanchnic vessels. World J Surg 2005;29:1122–1126.
13. Seyama Y, Kubota K, Kobayashi T, et al. Two-stage pancreatoduodenectomy with external drainage of pancreatic juice and omental graft technique. J Am Coll Surg 1998;187:103–105.

Prognostic Value of Tumor Architecture, Tumor-Associated Vascular Characteristics, and Expression of Angiogenic Molecules in Pancreatic Endocrine Tumors

Yu Takahashi,[1,3] Yuri Akishima-Fukasawa,[1] Noritoshi Kobayashi,[1] Tsuyoshi Sano,[2] Tomoo Kosuge,[2] Yuji Nimura,[3] Yae Kanai,[1] and Nobuyoshi Hiraoka[1]

Abstract **Purpose:** It is difficult to predict the biological behavior of pancreatic endocrine tumors (PETs). Our aim was to evaluate the prognostic significance of certain variables in PETs.

Experimental Design: The following variables were examined in 37 patients with PETs and then compared with other clinicopathologic characteristics: histologic tumor structure; microvessel density (MVD) measured by three different methods, including a unique method involving calculation of solid area MVD; endothelial proliferation; and the immunohistochemical expression of vascular endothelial growth factor-A and CXC chemokine CXCL-12. Intratumoral vascular structures were analyzed by double immunofluorescence using 30-μm-thick sections.

Results: The presence of focal and intensive solid growth of tumor cells (large solid nests; $P = 0.003$), low solid area MVD ($P = 0.002$), a high endothelial cell proliferation index (EPI; $P = 0.005$), and high expression of CXCL-12 in PET cells ($P = 0.018$) were significant unfavorable prognostic indicators. The predominant structure of the overall tumor histology and the expression of vascular endothelial growth factor-A did not separate aggressive PETs. In areas of focal solid growth, tumor-associated blood vessels had obviously low MVD and high EPI, and their structures were poorly formed with highly abnormal features, in comparison with other areas. High expression of CXCL-12 in tumor cells was significantly associated with variables representing tumor growth, hematogenous tumor spread, low MVD, high EPI, and the presence of large solid nests.

Conclusions: This study has provided novel findings on the prognostic features of tumor architecture and tumor-associated angiogenesis in PETs. CXCL-12 is the first candidate molecule in association with neoangiogenesis in PETs.

Pancreatic endocrine tumors (PETs) are uncommon neoplasms, and their prognostication is difficult when based purely on the histologic architecture and cytologic features of the tumor. Only the presence of distant metastases and local invasion to surrounding organs is the definitive criterion of malignancy (1–3). During the last few decades, various prognostic variables representing the proliferative or invasive ability of tumor cells have been reported, such as tumor size, mitotic rate, Ki-67 proliferative index, and presence of vascular and perineural invasion (1–5). Other molecules have also been reported to be prognostic variables, such as cytokeratin 19 and CD99 (6, 7). The last WHO classification of PETs used some of these variables, in addition to conventional histopathologic tumor typing (1). However, this is still not enough for predicting the biological behavior of PETs because retrospective studies have shown that patients with PETs classified as "well-differentiated endocrine tumors," "benign tumors," or "tumors of uncertain behavior" sometimes suffer tumor recurrence or die of the disease (4, 6). To identify more reliable prognostic variables representing the biological characteristics of PETs, we analyzed their histologic structure, focusing especially on the solidness of the tumor growth pattern and attempted to classify them on this basis. At the same time, we examined the characteristics of intratumoral (i.t.) blood vessels, as these are closely associated with tumor architecture. In our experience, microvessel density (MVD) is lower in areas where tumor cells of PETs grow in a more solid pattern.

Normal endocrine tissues, including pancreatic islets of Langerhans and endocrine tumors, are characterized by high vascular density. In a murine pancreatic endocrine carcinoma model, RIP1-Tag2 transgenic mice expressing the SV40 T antigen in insulin-producing β cells, the tumor vasculature increases, and

Authors' Affiliations: [1]Pathology Division, National Cancer Center Research Institute; [2]Division of Hepatobiliary and Pancreatic Surgery, National Cancer Center Hospital, Tokyo, Japan; and [3]Division of Surgical Oncology, Department of Surgery, Nagoya University Graduate School of Medicine, Nagoya, Japan

Received 6/12/06; revised 10/5/06; accepted 10/18/06.

Grant support: Ministry of Health, Labor, and Welfare of Japan grant-in-aid for Third-Term Comprehensive 10-Year Strategy for Cancer Control and Ministry of Education, Culture, Sports, Science, and Technology of Japan grant-in-aid for Scientific Research.

The costs of publication of this article were defrayed in part by the payment of page charges. This article must therefore be hereby marked *advertisement* in accordance with 18 U.S.C. Section 1734 solely to indicate this fact.

Note: Supplementary data for this article are available at Clinical Cancer Research Online (http://clincancerres.aacrjournals.org/).

Requests for reprints: Nobuyoshi Hiraoka, Pathology Division, National Cancer Center Research Institute, 5-1-1 Tsukiji, Chuo-ku, Tokyo 104-0045, Japan. Phone: 81-3-3542-2511; Fax: 81-3-3248-2463; E-mail: nhiraoka@gan2.res.ncc.go.jp.

doi:10.1158/1078-0432.CCR-06-1408

vascular morphology become abnormal during multistep carcinogenesis (8, 9). Tumor-associated blood vessels in various human cancers are structurally and functionally abnormal, showing increased permeability, delayed maturation, and potential for rapid proliferation (10, 11). The vessel defects may also facilitate hematogenous spread of tumor cells (12). Angiogenesis is essential for tumor growth and also plays an important role in hematogenous spread (13, 14). Measurement of MVD using immunohistochemistry is a widely used method for measuring angiogenic activity. Numerous studies have shown that elevated MVD is a significant predictive indicator of poor survival (13, 15). In human PETs, however, some recent studies have shown that low MVD is an unfavorable prognostic factor (16, 17), whereas others have suggested that MVD is not a predictive indicator of survival (18, 19). Thus, the relationship between MVD and biological behavior in human PETs is still controversial, although high MVD does not seem to be an unfavorable prognostic factor. It has been shown that angiogenic factors in many kinds of human cancers are related to metastatic dissemination, tumor aggressiveness, and short patient survival (20–22). Only vascular endothelial growth factor-A (VEGF-A) has been studied in human PETs, although there is still no evidence that it contributes to malignancy or patient survival (16–18). No attempt has been made to assess the prognostic value of angiogenic factors other than VEGF-A in PETs.

The aim of the present study was to investigate histologic tumor architecture, tumor-associated angiogenesis, and expression of angiogenic molecules in a series of resected PETs and to evaluate the potential prognostic significance of these variables.

Materials and Methods

Patients and samples. This study was approved by the Ethics Committee of the National Cancer Center, Tokyo, Japan. Clinical and pathologic data and the specimens used for immunohistochemical analysis were obtained through a detailed retrospective review of the medical records of all 37 Japanese patients with PETs who had undergone initial surgical resection between 1981 and 2004 at the National Cancer Center Central Hospital, Japan. The median age of the patients at surgery was 55 years (range, 18-81 years; mean, 52.9 years). None of the patients had received prior therapy and underwent potentially curative resection: pancreatoduodenectomy in 19 cases, distal pancreatectomy in 12 cases, tumor enucleation in 4 cases, and total pancreatectomy in 2 cases. Tumors were classified according to the WHO classification (1) into the following groups: benign well-differentiated endocrine tumors (referred to as WHO-1 in this report), well-differentiated endocrine tumors of uncertain behavior (WHO-2), well-differentiated endocrine carcinoma (WHO-3), and poorly differentiated endocrine carcinoma (WHO-4). Follow-up was available in all cases and ranged from 2 to 275 months (median, 46.8 months; mean, 65.2 months). During the follow-up period, nine patients presented with evidence of disease progression as liver metastasis, and two of them presented with evidence of local recurrence. The latest survival data were collected on December 31, 2004. The total survival rate was 78% at 5 years and 65% at 10 years. The clinicopathologic features of the patients are summarized in Table 1. Eight variables (large tumor size, presence of invasion to surrounding organs, presence of lymph node metastasis, presence of hematogenous metastasis, presence of vascular invasion, presence of perineural invasion, absence of functional hormone syndrome, and high Ki-67 index) had been reported to be unfavorable prognostic factors (1, 2). In our series, all these variables except "absence of functional hormone syndrome" were closely correlated with short survival (Table S1).

For histopathologic examinations, all tissue specimen was cut to make sections. Four-micrometer formalin-fixed, paraffin-embedded sections were prepared and stained with H&E. Vascular invasion was assessed by histopathologic examination, using H&E-stained tissue sections and sections stained for elastic fibers with Maeda's resorcin/fuchsin solution (Muto Pure Chemicals, Tokyo, Japan). With regard to the structural pattern of tumor histology, tumors were divided into four groups by the following criteria based on predominant architecture (Fig. 1A-D): grade 1, tumors consisting of small nests (with 1-5 tumor cells in the minor axis); grade 2, tumors consisting of moderate nests (with 6-10 tumor cells in the minor axis); grade 3, tumors consisting of large solid nests (with ≥11 tumor cells in the minor axis); and grade 4, tumors showing a diffuse growth pattern. The ratio of each solid grade was determined each tumor area in middle-power view and was calculated for the entire tumor area. Then the predominant grades were determined for each PET. PET with large solid nests was defined if there was at least a large solid nest in the tumor, regardless of the overall solid grading. Grading was carried out by two observers independently.

Immunohistochemistry. Immunohistochemistry was done on the formalin-fixed, paraffin-embedded tissue sections using the avidin-biotin complex method as described previously (23). We used 4-μm-thick sections of representative blocks with antibodies against the

Table 1. Summary of patients' demographics

Variables	WHO-1 (n = 6)	WHO-2 (n = 14)	WHO-3 (n = 15)	WHO-4 (n = 2)	Total
Sex (male/female)	2/4	6/8	6/9	1/1	15/22
Median age (y)	58.5	55.5	52	30	55
Functional hormone syndrome*	0	2	2	0	4
Mean tumor size (cm)	1.2	3.6	6.4	10.0	4.7
Invasion to surrounding organs	0	0	10	2	12
Lymph node metastasis	0	0	13	2	15
Hematogenous metastasis†	0	1	8	1	10
Vascular invasion	0	4	13	2	19
Perineural invasion	0	3	10	2	15
Ki-67 labeling index >5	0	4	10	2	16
Follow-up					
Alive and well without disease	5	13	7	1	26
Alive with disease	0	0	3	0	3
Dead of disease	0	1	4	1	6
Dead of other cause	1	0	1	0	2

*Four patients showed the clinical manifestation associated with hypersecretion of insulin in two cases: glucagon in one and gastrin in another.
†Tumor metastasized to liver or other organs by hematogenous spreading before and/or after the surgical resection of PETs.

following: chromogranin A (poly; 1:500), synaptophysin (poly; 1:50), neuron-specific enolase (BBS/NC/VI-H14; 1:100), CD31 (JC/70A; 1:50), CD34 (QBEnd 10; 1:100), Factor VIII (poly; 1:1000), α-smooth muscle actin (α-SMA; 1A4; 1:50), and Ki-67 (MIB-1; 1:100) from DAKO (Glostrup, Denmark); CD56 (NCC-Lu-243; 1:50) from Nippon Kayaku (Tokyo, Japan); VEGF-A (poly; 1:100) from Santa Cruz Biotechnology (Santa Cruz, CA); and CXCL-12 (79018; 1:50) from R&D Systems, Inc. (Minneapolis, MN). As a brief description, the sections were deparaffinized and rehydrated. After blocking of endogenous peroxidase with methanol containing 0.3% H_2O_2, the sections were autoclaved at 121°C for 10 min in citrate buffer (10 mmol/L sodium citrate, pH 6) for antigen retrieval. After blocking with normal goat serum, the sections were reacted overnight with appropriately diluted primary antibodies. The sections were then reacted sequentially with biotin-conjugated anti-mouse immunoglobulin G antibodies (Vector Laboratories, Burlingame, CA) and Vectastain Elite ABC reagent (Vector Laboratories). For staining VEGF-A, the sections were boiled at 95°C for 10 min for antigen retrieval. Diaminobenzidine was used as the chromogen, and the nuclei were counterstained with hematoxylin. For semiquantitative assessments of the immunohistochemical results for VEGF-A and CXCL-12, cytoplasmic staining intensity and the proportion of positive tumor cells were recorded. A staining index (with a value of 0-9) was calculated as the product of staining intensity (0-3) and area of positive staining (0, <1%; 1, 1-10%; 2, 10-50%; 3, >50%; ref. 23). The upper quartile was used as the cutoff point. The Ki-67 labeling index was determined as described previously (23). Immunohistochemical double staining for CD34 and Ki-67 was also done as described previously (24). Initially, Ki-67 was stained and visualized with diaminobenzidine as a brown-colored chromogen, followed by detachment of antibodies; then secondary immunohistochemistry was done to detect CD34; and the reaction product was visualized with VIP as a purple-colored chromogen (Vector Laboratories).

Evaluation of i.t. MVD. For evaluation of i.t. MVD, microvessels were detected by morphologic observation and immunohistochemical labeling with the endothelial markers CD31, CD34, and Factor VIII. In our preliminary study, three different markers detected endothelial cells similarly. CD34 showed the strongest intensity among them and could detect endothelial cells easily, but sometimes, it labeled fibroblasts that could be easily distinguished from vascular endothelial cells by their histology. Factor VIII showed the weakest staining intensity among them. Then we used CD34 for MVD assay and CD31 for immunofluorescence double staining. All independent CD34-positive vessel structures were counted, irrespective of the presence of an identifiable lumen. For assessment of MVD, we used three different methods as follows. Average MVD (Av-MVD) was analyzed by selecting 10 randomized fields per tumor at a magnification of ×200 (0.95 mm^2 per field), and the number of CD34-positive vessel structures in each field was counted. The mean number of vessels was then calculated after exclusion of the lowest and highest values measured (16). Hotspot MVD was assessed by a modification of the Weidner technique (21). The H&E-stained tissue sections were screened, and three areas with the most intense vascularization were selected at low magnification. We then counted CD34-positive vessels at a magnification of ×200, and the average counts for the three fields were calculated. For solid area MVD (S-MVD), the H&E-stained tissue sections were screened, and we selected three areas showing the most solid growth pattern of tumor cells, which often contained large solid nests or a diffuse growth pattern. Then CD34-positive vessels at a magnification of ×200 were counted in each corresponding area. The average counts of the three fields was calculated and defined as the S-MVD. Two observers, having no access to the patient data, evaluated independently MVD, morphometrical vessel characters, and proliferating endothelial cells described below. Their final value was the average of the value counted by the two observers. To assess intraobserver reproducibility, several tissue sections were counted thrice by each observer. To assess interobserver reproducibility, 10 data counted by each observer for the same tumor were compared (16).

Immunofluorescence double staining. Immunofluorescence double staining was done on 30-μm-thick, formalin-fixed, paraffin-embedded tissue sections as described previously (24), with some modifications. All antibodies were diluted in 0.2% Triton X-100 and 5% skim milk in TBS-T. α-SMA antigens were stained by the CSA system (DAKO) with our modification, and then CD31 was stained with CSAII (DAKO). Reaction time for the primary and secondary antibodies was extended to overnight and 1 h, respectively. After reaction with biotin-conjugated tyramide solution, the sections were incubated with Texas Red–conjugated avidin (1:200) for 1 h at room temperature. After detaching the antibodies by acid treatment (100 mmol/L glycine/HCl, pH 2.2) for 2 h, the sections were stained with CD31 using CSAII according to the manufacturer's instructions with modifications. Just after reaction of the sections with FITC-conjugated tyramide, the sections were washed and mounted with Vectashield mounting medium (Vector Laboratories). Immunostained tissue sections were analyzed with a confocal microscope (LSM5 Pascal; Carl Zeiss Jena GmbH, Jena, Germany) equipped with a 15-mW Kr/Ar laser. The confocal files were saved, compiled, and fused to make three-dimensional pictures.

To estimate the branching frequency of blood vessels, 12 randomized fields were selected for each tumor at a magnification of ×200. The distance of blood vessels between the closest two branches in each field was measured, and the mean length for each tumor was calculated, which we termed the unbranched vessel length. To estimate variability in the luminal diameter of blood vessels, 12 randomized fields were selected for each tumor at a magnification of ×400. The maximum and minimum luminal diameters of blood vessels between the closest two branches in each field were measured, and the average of the difference in diameter was calculated. To evaluate abnormality of blood vessels showing irregular vessel wall shapes and distortion, i.t. vessels were divided into five categories: category 1 corresponded to regular vessels in normal islets of Langerhans, category 5 corresponded to the most severely changed vessels as shown in Fig. 4G to I, and categories 2 to 4 corresponded to vessels with mild to severe abnormalities between categories 1 and 5.

Endothelial cell proliferation in i.t. blood vessels. To evaluate the proliferation of endothelial cells, tumor tissues that had been double stained for Ki-67 and CD34 were assessed by modified previous methods (25, 26). Fifty randomized fields at a high magnification (×400) were selected for each tumor, and we counted the number of CD34-expressing endothelial cells with Ki-67–positive nuclei in each field, then the total amount was defined as the endothelial cell proliferation (ECP). The ECP proliferation index (EPI) was defined as the ECP divided by the Av-MVD that was assessed in the same fields because MVD was different in each tumor.

Statistical analysis. Statistical analyses were done with StatView-J 5.0 software (Abacus Concepts, Berkeley, CA) and SPSS statistical software version 12.0 (SPSS, Inc., Chicago, IL). Association between categorical variables was examined by Fisher's exact probability test. Mann-Whitney nonparametric tests were used to compare categorical with continuous tumor variables when there were two categories, whereas Kruskal-Wallis nonparametric tests were used instead when there were more than two categories. Differences at $P < 0.05$ were considered significant. Survival rates were computed by the Kaplan-Meier method and compared by the log-rank test.

Results

The clinicopathologic characteristics of the 37 patients with PETs are described in Materials and Methods and Table 1.

Histologic structural pattern. The histologic pattern of tumor growth was studied to clarify whether it could predict tumor behavior. Initially, we classified PETs into four categories based on the solidness of the predominant tumor histology, ranging from grade 1, which was least solid, to grade 4, which showed

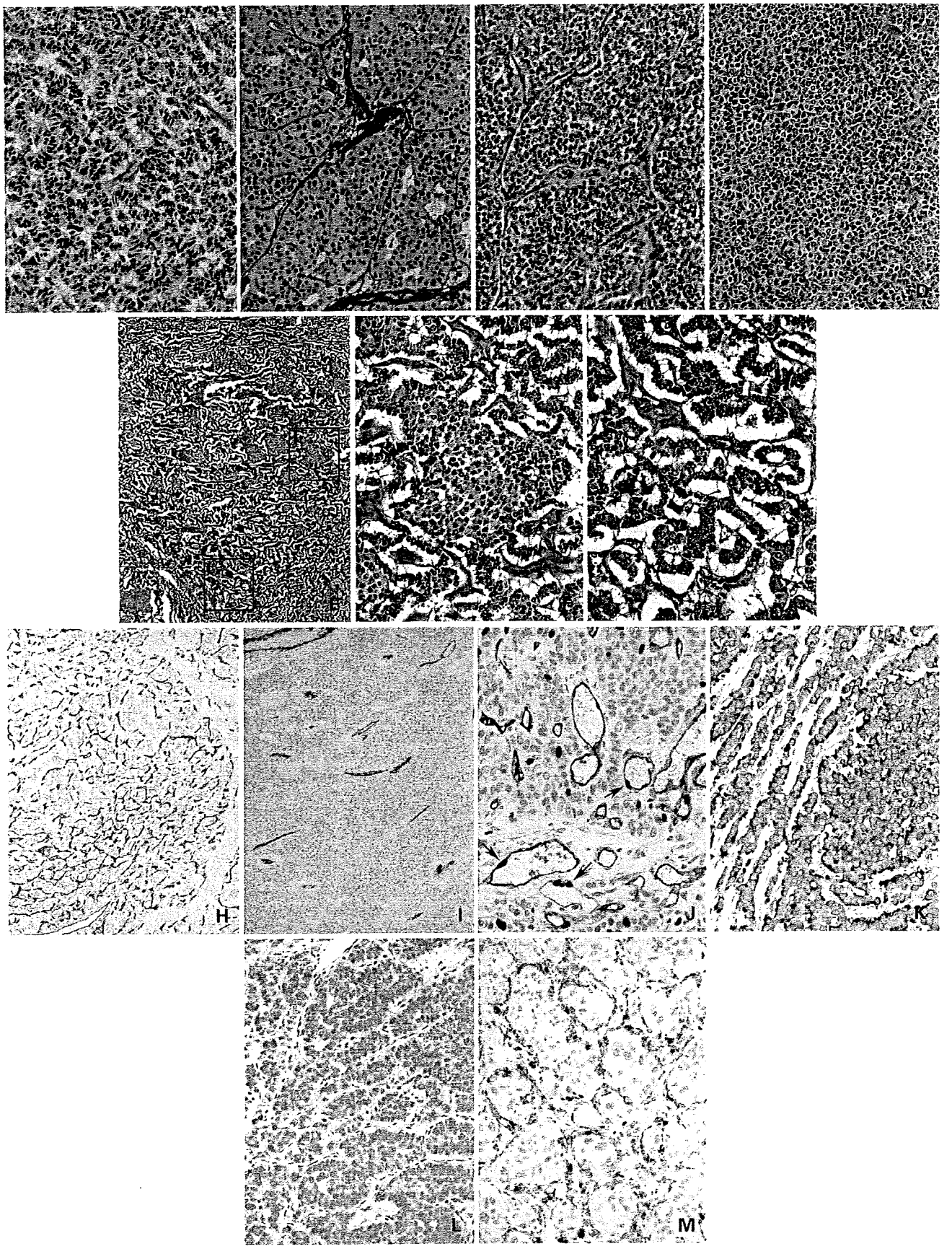
D
H
H
I
J
K
L
M

the most solid and diffuse growth (Fig. 1A-D). Most of the PETs were classified as grade 1 (19 of 37; Table 2), which included tumors with a predominant histologic structure showing a thin trabecular, gyriform, or pseudoglandular pattern. All of the grade 3 PETs belonged to WHO-3, and grade 4 PETs belonged to WHO-4. There was no significant correlation between any of the grades and disease-free survival, but disease-free survival became closely correlated when grade 1 and 2 PETs were combined (Fig. 2A).

We then selected PETs that had a "large solid nest" defined as the presence of ≥11 tumor cells in the minor axis, independent of the overall tumor histologic pattern (Fig. 1E-G). Twenty PETs had large solid nests, including five grade 1 PETs, seven grade 2 PETs, and eight grade 3 and grade 4 PETs (Table 2). Interestingly, all the patients that suffered tumor recurrence had PETs with large solid nests, and all the patients without large solid nests remained disease-free. The presence of large solid nests was a significant factor correlated with disease-free survival (log-rank test, $P = 0.003$; Fig. 2B). The presence of large solid nests was significantly correlated with tumor size ($P = 0.008$), invasion to surrounding organs ($P = 0.002$), lymph node metastasis ($P = 0.018$), hematogenous metastasis ($P = 0.0006$), vascular invasion ($P = 0.0002$), and Ki-67 index ($P = 0.007$; Table S1).

MVD. The relationship between MVD and biological behavior in human PETs is controversial (16–18), probably as a result of how MVD is counted. To clarify whether MVD is related to tumor behavior and to select the best way to count MVD, we tried to measure MVD of PETs using three different counting methods (Materials and Methods; Fig. 1H and I): Av-MVD, hotspot MVD, and S-MVD. Av-MVD ranged from 59.4 to 423.5 vessels per field (mean, 189.1; median, 167.6); hotspot MVD ranged from 132.3 to 625.0 vessels per field (mean, 288.3; median, 268.0); and S-MVD ranged from 30.0 to 468.3 vessels per field (mean, 161.5; median, 132.3). Av-MVD and S-MVD decreased according to the progression of PETs by the WHO classification, and this was statistically significant (Kruskal-Wallis test: Av-MVD, $P = 0.010$; S-MVD, $P = 0.003$; Fig. 3A and Fig. S1). Hotspot MVD did not show apparent differences among the WHO classes ($P = 0.500$; Fig. S1). When all the PETs were divided into two groups based on median MVD, the high MVD group showed longer patient survival than the low MVD group (Fig. 3B and Fig. S1). The difference was clearer for S-MVD (log-rank test, $P = 0.002$), and the high S-MVD group included no patients with recurrent tumors. S-MVD was significantly correlated with tumor size ($P = 0.002$), invasion to surrounding organs ($P = 0.001$), lymph node metastasis ($P = 0.0006$), hematogenous metastasis ($P = 0.0004$), vascular invasion ($P < 0.0001$), perineural invasion ($P = 0.007$), and Ki-67 index ($P = 0.0002$; Table S1).

Vascular ECP. The dynamics of neoangiogenesis in PETs was assessed by ECP (Materials and Methods; Fig. 1J). ECP ranged from 0 to 26 (mean, 7.59; median, 7). Surprisingly, the ECP was higher in low S-MVD tumors ($P = 0.011$; Fig. 3C). EPI (Materials and Methods; range, 0.00-0.27; mean, 0.057; median, 0.038) was also higher in PETs with low S-MVD and was significantly correlated with WHO classification (Kruskal-Wallis test, $P = 0.001$; Fig. 3D). When patients were divided into two groups by the median EPI, the high EPI group showed significantly shorter disease-free survival than the low EPI group (log-rank test, $P = 0.005$; Fig. 3E). EPI was significantly correlated with tumor size ($P < 0.0001$), invasion to surrounding organs ($P = 0.005$), lymph node metastasis ($P = 0.020$), hematogenous metastasis ($P = 0.003$), vascular invasion ($P < 0.0001$), and Ki-67 index ($P = 0.0008$; Table S1).

Table 2. Relationship between histologic structural grades or tumors with large solid nests and WHO classification of pancreatic endocrine tumors

	Grade 1	Grade 2	Grade 3	Grade 4	Total cases
WHO-1	4 (1)	2 (2)	0	0	6 (3)
WHO-2	11 (2)*	3 (1)	0	0	14 (3)
WHO-3	4 (2)**	5 (4)*	6 (6)****	0	15 (12)
WHO-4	0	0	0	2 (2)*	2 (2)
Total	19 (5)	10 (7)	6 (6)	2 (2)	37 (20)

NOTE: The numbers of patients with PET having large solid nests are in parentheses.
*n, number of asterisks (*) represent numbers of patients with PET recurrence.

Vascular characteristics. We then analyzed the structures of blood vessels to determine whether blood vessels change to poorly formed vessels with multiple abnormalities, in association with tumor progression. We analyzed 9 PETs with high S-MVD and 13 PETs with low S-MVD that were available for immunofluorescence analysis using 30-μm-thick tissue sections stained for CD31 and α-SMA. There were fine mesh-like structures consisting of smooth, thin, and relatively regular vessels in tumors with high S-MVD (Figs. 1H and 4D-F). The rough structure of the vasculature in tumors with high S-MVD was similar to the vascular features of normal islets of Langerhans (Fig. 4A-C), although the vessels in the tumors were thick, and their detailed structures were irregular. In contrast, the vasculature in PETs with low S-MVD was less branched and relatively straight (Fig. 4J), consisting of thicker, more irregularly shaped and often distorted vessels (Figs. 1I, 4G-I and 4L). In high-power view, instead of mature branches, there were many very small and irregular buds on the vessels, which showed highly abnormal features (Fig. 4I). α-SMA–positive cells covered these irregular buds. The luminal diameter of vessels was more variable in PETs with low S-MVD than in PETs with high S-MVD (Fig. 4K). Almost all the i.t. blood vessels were covered by α-SMA–positive mural cells, although α-SMA–positive multiple layers were often observed in PETs with low S-MVD. These findings indicated that i.t. blood vessels in PETs with low S-MVD were poorly formed blood vessels with multiple abnormalities,

Fig. 1. *A* to *D*, histologic structural grading of PETs based on the degree of solid growth of tumor cells in the predominant architecture. Grade 1 tumor consists of small nests (*A*). Grade 2 tumor consists of moderate nests (*B*). Grade 3 tumor consists of large solid nests (*C*). Grade 4 tumor grows in a diffuse solid pattern (*D*). *E* to *G*, large solid nests. Tumor cells proliferate predominantly in a trabecular pattern and sometimes form large solid nests focally in low-power view (*E*). Middle-power view of large solid nests (*F*) and trabecular pattern (*G*). *H* to *M*, immunohistochemistry. CD34-labeled endothelial cells are detected in PET with high MVD (*H*) and in PET with low MVD (*I*) in low-power view. *J*, CD34 (*purple*) is expressed in vascular endothelial cells, and nuclei of proliferating cells are labeled by Ki-67 (*brown*) in high-power view. Arrows, proliferating endothelial cells. *K*, VEGF-A stained in cytoplasm of PET cells in middle-power view. CXCL-12 stained in PET cells (*L*) and blood vessels (*M*) in middle-power view.

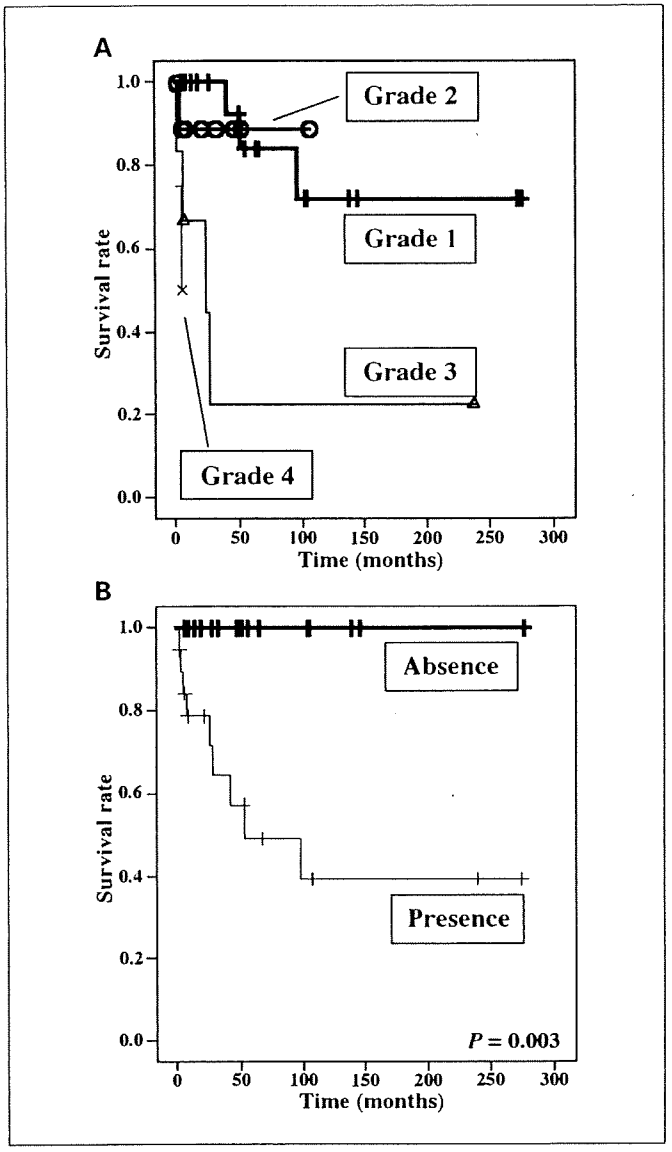

Fig. 2. Kaplan-Meier survival curves of the 37 patients with PETs. *A*, PETs are classified by predominant histological structures into four grades. There was no significant correlation between this classification and disease-free survival. *B*, PETs are divided by the presence or absence of large solid nests. Patients with PETs showing large solid nests had significantly shorter disease-free survival (log-rank test, $P = 0.003$).

whereas blood vessels in PETs with high S-MVD still had the characteristics of endocrine organs.

Expression of VEGF-A and CXCL-12 in PETs. To assess the angiogenic factors in PETs, we analyzed the expression of VEGF-A and CXCL-12 in tumor cells and i.t. blood vessels by immunohistochemistry (Fig. 1K-M). CXCL-12 is known to be a CXC chemokine involved in the recruitment of circulating endothelial progenitor cells from bone marrow to the target organs (27, 28). High expression of CXCL-12 in tumor cells was significantly correlated with high EPI ($P = 0.020$; Table 3) and low S-MVD ($P = 0.0006$; Table 3), although expression of CXCL-12 in i.t. blood vessels and VEGF-A expressed in tumor cells did not closely correlate with EPI and S-MVD (Table 3). High expression of VEGF-A in tumor cells was significantly correlated with high expression of CXCL-12 in i.t. blood vessels ($P < 0.0001$) but not to other clinicopathologic variables, including expression of CXCL-12 in tumor cells (Table 3). A high value of CXCL-12 in the tumor was significantly correlated with marked vascular invasion ($P = 0.0006$), the presence of hematogenous metastasis ($P = 0.006$), large tumor size ($P = 0.035$), a high Ki-67 index ($P = 0.006$), and the presence of large solid nests ($P = 0.018$). Furthermore, PETs having high amounts of CXCL-12 in the tumor cells were closely correlated with a shorter disease-free patient survival rate (log-rank test, $P = 0.018$; Fig. 3F).

Discussion

In this study, we found a new histologic marker for predicting the biological behavior of PETs (i.e., "the presence of focal large solid nests"), which is independent of the predominant histologic structure. Then we measured S-MVD and showed a close correlation between low MVD and an unfavorable prognosis in PETs. Paradoxically, i.t. vessels of PETs with a high MVD showed low EPI and vice versa. Morphometric analysis showed that blood vessels in PETs with low MVD were more poorly formed and had more irregular and abnormal features, whereas blood vessels in PETs with high MVD showed relatively regular mesh-like features similar to vessels in normal islets of Langerhans. These findings imply that a high MVD seems to be a characteristic of blood vessels in islets of Langerhans, and that EPI can be a hallmark of angiogenic activity in tumor-associated blood vessels in PETs. Our data also suggest that EPI and S-MVD are predictors of the biological behavior of PETs. We analyzed angiogenic factors in PETs and found that high EPI and low MVD were significantly correlated with high expression of CXCL-12 in tumor cells but not with the expression of CXCL-12 in i.t. blood vessels and VEGF-A. Combined with the data for the relationship between CXCL-12 and other variables, it is suggested that CXCL-12 produced in tumor cells is involved in the angiogenesis of tumor-associated vessels and hematogenous spread as well as proliferation of tumor cells and thus may contribute to the aggressiveness of PETs. CXCL-12 is the first molecule to be highlighted as a possible angiogenic factor playing important roles in the neoangiogenesis of PETs. Thus, we have provided novel data on the prognostic features of tumor architecture and tumor-associated angiogenesis in PETs.

In contrast to the predominant histologic structures, the presence of focal large solid nests delineated PETs with aggressive behavior. Even in grade 1 and 2 PETs, patients with large solid nests had significantly shorter disease-free survival than patients without them ($P = 0.024$). Interestingly, metastatic PETs showed almost the same histologic architecture as the original pancreatic tumors and were not occupied by tumor cells with solid growth. These findings suggest that tumor cells in large solid nests are not more progressed or more malignant than their origin, and that the presence of large solid nests represents the potential for tumor malignancy.

By comparing three methods for evaluation of MVD, we found that the best variable for predicting the representative biological characteristics of PETs was S-MVD. This seems reasonable because in PETs, we showed that a focal tumor structure showing the most solid growth represents the behavior of the tumor as a whole. Morphometric analysis also showed that irregularity and abnormality of i.t. blood vessels were associated with tumor growth pattern where the vessels were present. These findings

imply that tumor architecture is closely correlated with local vessel formation, and that tumor cells and blood vessels seem to be a pair of components within a single structure.

Our results indicate that EPI and MVD can be prognostic variables in patients with PETs. Abnormal tumor-associated blood vessels tend to grow rapidly (10), consistent with the fact that PETs with more poorly formed blood vessels have a high EPI. EPI is also significantly correlated with hematogenous spread (vascular invasion, $P < 0.0001$; hematogenous metastasis, $P = 0.003$) and survival ($P = 0.005$) in PETs. Recently, similar results were indicated in the other tumor by Stefansson et al. That is, increased vascular proliferation was associated with aggressive features of tumors and was an independent prognostic factor in endometrial carcinoma (26).

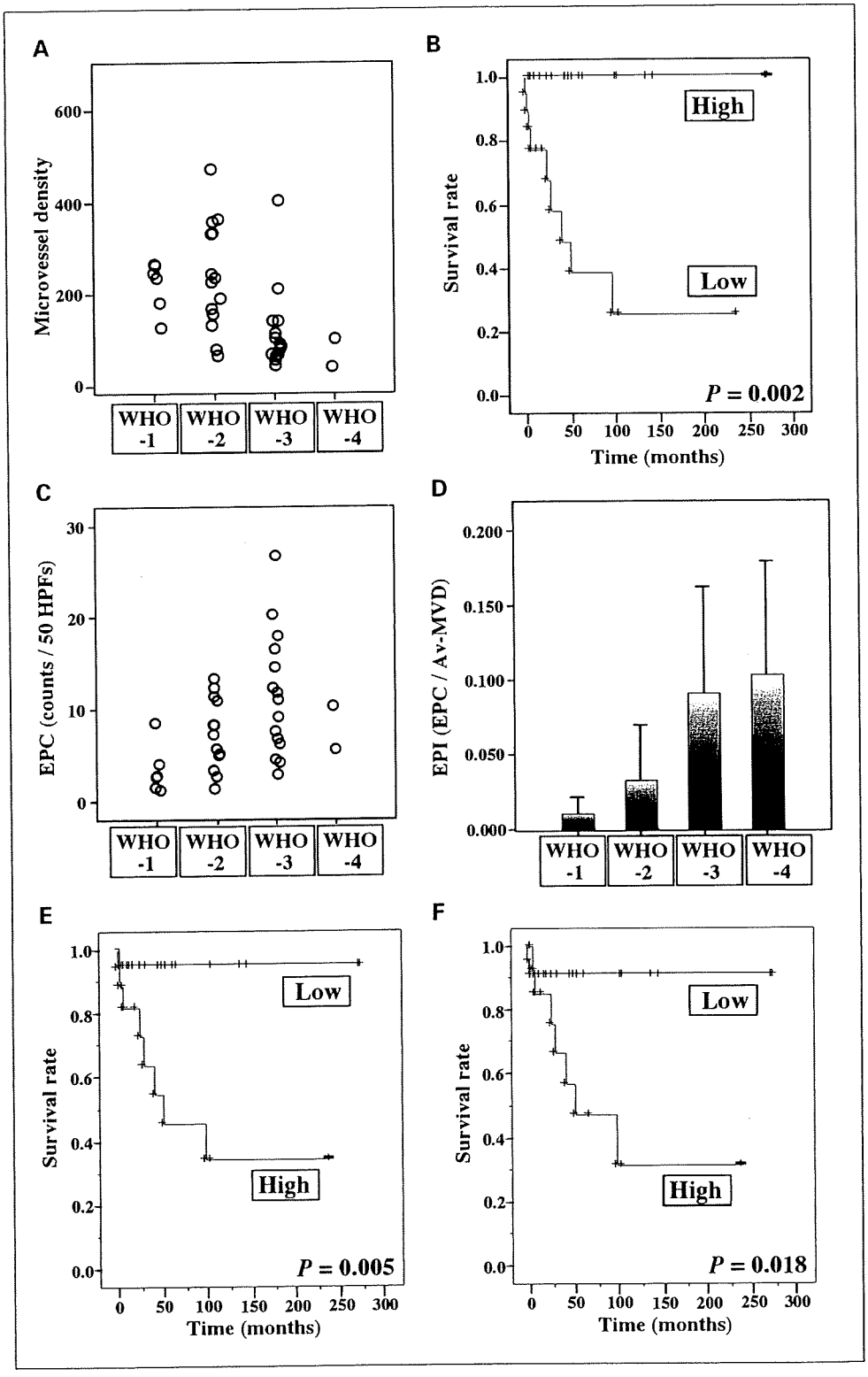

Fig. 3. *A*, *C*, and *D*, relationship between vascular index and WHO classification. *B*, *E*, and *F*, Kaplan-Meier survival curves of 37 patients with PETs. *A*, S-MVD significantly decreased according to progression of PETs in terms of the WHO classification (Kruskal-Wallis test, $P = 0.003$). *B*, patients were divided into two groups by median S-MVD. The high S-MVD group showed significantly longer survival than the low S-MVD group (log-rank test, $P = 0.002$). *C*, EPC significantly increased according to progression of PETs in terms of the WHO classification (Kruskal-Wallis test, $P = 0.019$). *D*, EPI significantly increased according to progression of PETs in terms of the WHO classification (Kruskal-Wallis test, $P = 0.001$). *E*, patients were divided into two groups by median EPI. The high EPI group showed significantly shorter survival than the low EPI group (log-rank test, $P = 0.005$). *F*, patients were divided into two groups by the quartile value of CXCL-12 expressed in the tumor cells. Patients with PETs showing high expression of CXCL-12 in the tumor cells had significantly shorter survival than those whose tumors showed low expression (log-rank test, $P = 0.018$).

What kinds of molecules are involved in tumor-associated angiogenesis in PETs? It has been reported that in many kinds of cancers VEGF produced in tumor cells accelerates tumor-associated angiogenesis, leading to tumor growth and a high frequency of hematogenous tumor cell spread (14). VEGF-A expression in PETs is reported to be not closely correlated with MVD (16, 18) or to be closely correlated with high MVD (17). In our series, there was no close correlation of VEGF-A expression with growth of blood vessels, hematogenous spread, or tumor growth in PETs, but with high expression of CXCL-12 in i.t. blood vessels. CXCL-12 has chemotactic activity for leukocytes (28) and stem cells (29). Grunewald et al. reported that VEGF-A induces adult neovascularization mediated by CXCL-12 expression in the microenvironment. VEGF-A recruits endothelial progenitor cells from the bone marrow to the blood and induces expression of CXCL-12, which traps and correctly positions endothelial progenitor cells around growing vessels in tissues (27). Our study suggested that VEGF-A induced the expression of CXCL-12 in tumor vessels, although such events did not lead to tumor-associated neoangiogenesis in PETs. In contrast, high EPI was closely correlated with high CXCL-12 produced in tumor cells ($P = 0.020$). High expression of CXCL-12 in tumor cells was also positively correlated with variables of hematogenous tumor spread (versus vascular invasion, $P = 0.0006$; versus hematogenous metastasis, $P = 0.006$) and tumor growth (versus tumor size, $P = 0.035$; versus Ki-67 index, $P = 0.006$) and also with shorter patient survival ($P = 0.018$). These findings suggest that CXCL-12 produced in tumor cells is involved in the aggressive features of tumor mediated by neoangiogenesis and tumor growth. Orimo et al. reported that carcinoma-associated fibroblasts in breast cancer secrete CXCL-12, which promotes the growth of the tumor cells both directly

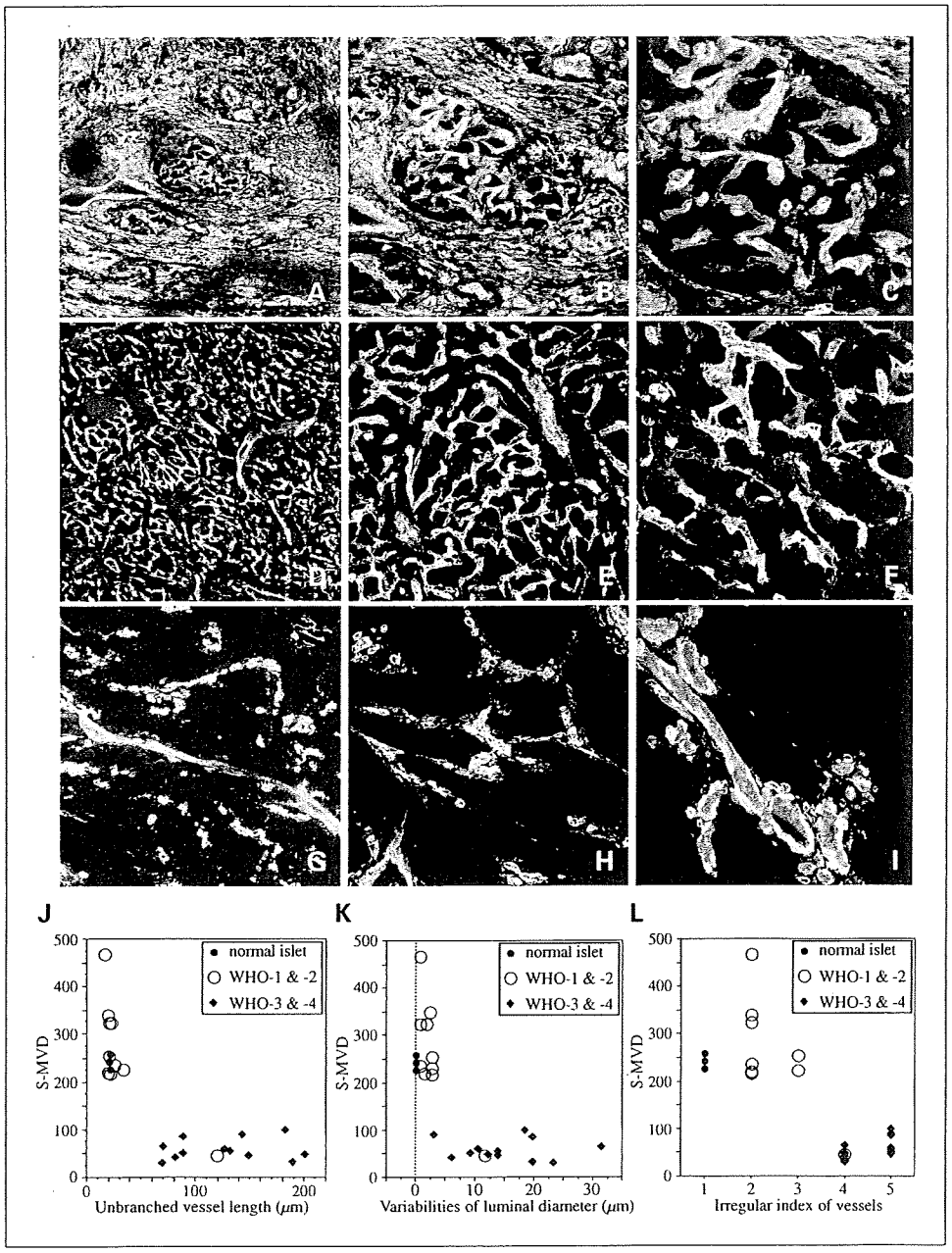

Fig. 4. Characterization of tumor-associated blood vessels in double immunofluorescence examination of CD31 (*green*) and α-SMA (*red*) using 30-μm-thick sections. Normal islet of Langerhans in low-power (*A*), middle-power (*B*), and high-power (*C*) view. PET with high S-MVD in low-power (*D*), middle-power (*E*), and high-power (*F*) view. PET with low S-MVD in low-power (*G*), middle-power (*H*), and high-power (*I*) view. *J* to *L*, morphometric analyses of PETs. I.t. blood vessels were examined for unbranched vessel length (*J*), variability of luminal diameter (*K*), and vessel irregularity (*L*).

Table 3. Relationship between clinicopathologic variables and VEGF-A or CXCL-12

Variables	*n*	VEGF-A			CXCL-12 in tumor cells			CXCL-12 in blood vessels		
		High (*n* = 19)	Low (*n* = 18)	*P*	High (*n* = 19)	Low (*n* = 18)	*P*	High (*n* = 19)	Low (*n* = 18)	*P*
Age (y)										
≤55	19	8	11	NS	8	11	NS	8	11	NS
>55	18	10	8		7	11		11	7	
Sex										
Female	22	13	9	NS	10	12	NS	13	9	NS
Male	15	5	10		5	10		6	9	
Functional hormone syndrome										
Absence	33	16	17	NS	14	19	NS	17	16	NS
Presence	4	2	2		1	3		2	2	
Tumor size (cm)										
<2	13	3	10	0.038	2	11	0.035	4	9	NS
≥2	24	15	9		13	11		15	9	
Invasion to surrounding organs										
Absence	25	12	13	NS	7	18	NS	15	10	NS
Presence	12	6	6		8	4		4	8	
Lymph node metastasis										
Absence	22	8	14	NS	6	16	NS	11	11	NS
Presence	15	10	5		9	6		8	7	
Hematogenous metastasis*										
Absence	27	12	15	NS	7	20	0.006	13	14	NS
Presence	10	6	4		8	2		6	4	
Vascular invasion										
Absence	18	6	12	NS	2	16	0.0006	9	9	NS
Presence	19	12	7		13	6		10	9	
Perineural invasion										
Absence	22	10	12	NS	7	15	NS	12	10	NS
Presence	15	8	7		8	7		7	8	
Ki-67 labeling index										
≤5	21	8	13	NS	4	17	0.006	9	12	NS
>5	16	10	6		11	5		10	6	
Histologic structural grades										
1 + 2	29	15	14	NS	10	19	NS	18	11	0.019
3 + 4	8	3	5		5	3		1	7	
Large solid nests										
Absence	17	7	10	NS	3	14	0.018	9	8	NS
Presence	20	11	9		12	8		10	10	
S-MVD										
High	18	7	11	NS	2	16	0.0006	10	8	NS
Low	19	11	8		13	6		9	10	
EPI										
High	18	11	7	NS	11	7	0.020	10	8	NS
Low	19	7	12		4	15		9	10	
VEGF-A										
High	18				10	8	NS	16	2	<0.0001
Low	19				5	14		3	16	
CXCL-12 in tumor cells										
High	15	10	5	NS				8	7	NS
Low	22	8	14					11	11	
CXCL-12 in vessels										
High	19	16	3	<0.0001	8	11	NS			
Low	18	2	16		7	11				

Abbreviation: NS, not significant.
*Tumor metastasized to liver or other organs by hematogenous spreading before and/or after the surgical resection of PETs.

and indirectly, and promotes neoangiogenesis by recruiting endothelial progenitor cells (30). Finally, high expression of CXCL-12 in tumor cells had a close correlation with the presence of large solid nests ($P = 0.018$). It is possible that CXCL-12 produced by tumor cells may mediate the formation of focal solid structures by a pair of solid growing tumor cells and their surrounding tumor-associated blood vessels with highly abnormal features. Furthermore, it is suggested that interrupting the angiogenic pathway mediated by CXCL-12 may provide a novel and efficient antiangiogenesis strategy for the treatment of PETs.

Acknowledgments

We thank Drs. Kazuaki Shimada, Yoshihiro Sakamoto, Hidenori Ojima, and Hiroki Ochiai for useful discussions and Kaoru Onozato, Yuko Yamauchi, Fumi Kaiya-Toshioka, Ayaka Miura, and Rie Itoh for their technical advice.

References

1. DeLellis RA, Lloyd RV, Heitz PU, Eng C. World Health Organization classification of tumours. Pathology and genetics of tumours of endocrine organs. Lyon: IARC Press; 2004. p. 175–208.
2. Solcia E, Capella C, Klöppel G. Tumors of the pancreas. Atlas of tumor pathology. 3rd series, fascicle 20. Washington (DC): Armed Forces Institute of Pathology; 1997.
3. Maderia I, Terris B, Voss M, et al. Prognostic factors in patients with endocrine tumours of the duodenopancreatic area. Gut 1998;43:422–7.
4. Hochwald SN, Zee S, Conlon KC, et al. Prognostic factors in pancreatic endocrine neoplasms: an analysis of 136 cases with a proposal for low-grade and intermediate-grade groups. J Clin Oncol 2002;20:2633–42.
5. Jorda M, Ghorab Z, Fernandez G, Nassiri M, Hanly A, Nadji M. Low nuclear proliferative activity is associated with nonmetastatic islet cell tumors. Arch Pathol Lab Med 2003;127:196–9.
6. Deshpande V, Castillo CF, Muzikansky A, et al. Cytokeratin 19 is a powerful predictor of survival in pancreatic endocrine tumors. Am J Surg Pathol 2004;28:1145–53.
7. Goto A, Niki T, Terada Y, Fukushima J, Fukayama M. Prevalence of CD99 protein expression in pancreatic endocrine tumors (PETs). Histopathology 2004;45:384–92.
8. Hanahan D, Folkman J. Patterns and emerging mechanisms of the angiogenic switch during tumorigenesis. Cell 1996;86:353–64.
9. Lopez T, Hanahan D. Elevated levels of IGF-1 receptor convey invasive and metastatic capability in a mouse model of pancreatic islet tumorigenesis. Cancer Cell 2002;1:339–53.
10. Jain RK. Molecular regulation of vessel maturation. Nat Med 2003;9:685–93.
11. Morikawa S, Baluk P, Kaidoh T, et al. Abnormalities in pericytes on blood vessels and endothelial sprouts in tumors. Am J Pathol 2002;160:985–1000.
12. Hashizume H, Baluk P, Morikawa S, et al. Openings between defective endothelial cells explain tumor vessel leakiness. Am J Pathol 2000;156:1363–80.
13. Ellis LM, Fidler IJ. Tumor angiogenesis. In: Mendelsohn J, Howley PM, Israel MA, et al. editors. The molecular basis of cancer. 2nd ed. Philadelphia: Saunders; 2001. p. 173–85.
14. Carmeliet P, Jain RK. Angiogenesis in cancer and other diseases. Nature 2000;407:249–57.
15. Poon RTP, Ng IOL, Lau C, et al. Tumor microvessel density as a predictor of recurrence after resection of hepatocellular carcinoma: a prospective study. J Clin Oncol 2002;20:1775–85.
16. Marion-Audibert AM, Barel C, Gouysse G, et al. Low microvessel density is an unfavorable histoprognostic factor in pancreatic endocrine tumors. Gastroenterology 2003;125:1094–104.
17. Couvelard A, O'Toole D, Turley H, et al. Microvascular density and hypoxia-inducible factor pathway in pancreatic endocrine tumours: negative correlation of microvascular density and VEGF expression with tumour progression. Br J Cancer 2005;92:94–101.
18. La Rosa S, Uccella S, Finzi G, Alvarello L, Sessa F, Capella C. Localization of vascular endothelial growth factor and its receptors in digestive endocrine tumors: correlation with microvessel density and clinicopathologic features. Hum Pathol 2003;34:18–27.
19. Tan G, Cioc AM, Perez-Montiel D, Ellison EC, Frankel WL. Microvascular density does not correlate with histopathology and outcome in neuroendocrine tumors of the pancreas. Appl Immunohistochem Mol Morphol 2004;12:31–5.
20. Folkman J. Clinical applications of research on angiogenesis. N Engl J Med 1995;333:1757–63.
21. Weidner N. Tumoural vascularity as a prognostic factor in cancer patients: the evidence continues to grow. J Pathol 1998;184:119–22.
22. Weidner N, Semple JP, Welch WR, Folkman J. Tumor angiogenesis and metastasis - correlation in invasive breast carcinoma. N Engl J Med 1991;324:1–8.
23. Takahashi Y, Hiraoka N, Onozato K, et al. Solid-pseudopapillary neoplasms of the pancreas in men and women: do they differ? Virchows Arch 2006;448:561–9.
24. Hiraoka N, Onozato K, Kosuge T, Hirohashi S. Prevalence of FOXP3$^+$ regulatory T cells increases during the progression of pancreatic ductal adenocarcinoma and its premalignant lesions. Clin Cancer Res 2006;12:5423–34.
25. Eberhard A, Kahlert S, Goede V, et al. Heterogeneity of angiogenesis and blood vessel maturation in human tumors: implications for antiangiogenic tumor therapies. Cancer Res 2000;60:1388–93.
26. Stefansson IM, Salvesen HB, Akslen LA. Vascular proliferation is important for clinical progress of endometrial cancer. Cancer Res 2006;66:3303–9.
27. Grunewald M, Avrahum I, Dor Y, et al. VEGF-induced adult neovascularization: recruitment, retention, and role of accessory cells. Cell 2006;124:175–89.
28. Bluel CC, Farzan M, Choe H, et al. The lymphocyte chemoattractant SDF-1 is a ligand for LESTR/fusin and blocks HIV-1 entry. Nature 1996;382:829–33.
29. Peled A, Petit I, Kollet O, et al. Dependence of human stem cell engraftment and repopulation of NOD/SCID mice on CXCR4. Science 1999;283:845–8.
30. Orimo A, Gupta PB, Sgroi DC, et al. Stromal fibroblasts present in invasive human breast carcinomas promote tumor growth and angiogenesis through elevated SDF-1/CXCL12 secretion. Cell 2005;121:335–48.

Pathology International 2007; **57**: 794–798 doi:10.1111/j.1440-1827.2007.02176.x

Case Report

Invasive biliary cystic tumor without ovarian-like stroma

Yuji Ishibashi,[1] Hidenori Ojima,[2] Nobuyoshi Hiraoka,[2] Tsuyoshi Sano,[3] Tomoo Kosuge[3] and Yae Kanai[2]

[1]Clinical Laboratory Division and [3]Hepatobiliary and Pancreatic Surgery Division, National Cancer Center Hospital and [2]Pathology Division, National Cancer Center Research Institute, Tokyo, Japan

Presented herein is a rare case of invasive biliary cystic tumor without an ovarian-like stroma, and the apparent sequence underlying its malignant transformation, which was identified on detailed histological examination. A 54-year-old woman was incidentally diagnosed as having a cystic tumor in segment VIII of the liver, and central bisegmentectomy was performed. Macroscopically the tumor measured 4.6 × 3.5 cm; and unilocular cystic and solid areas were seen on cut surface. Microscopically the tumor showed three types of neoplasia: adenoma and tubulopapillary adenocarcinoma in the cystic area, and invasive adenocarcinoma in the solid area. The relative area of the tumor occupied by each of these histological types was approximately 3%, 50% and 47%, respectively. Moreover, transitional zones between adenoma and tubulopapillary adenocarcinoma, and between tubulopapillary adenocarcinoma and invasive adenocarcinoma were noted. The immunohistochemical expression of Ki-67 and p53 increased gradually from adenoma through to tubulopapillary adenocarcinoma, and was highest in invasive adenocarcinoma. MUC1 was positive, and MUC2 and MUC5AC were both negative. No ovarian-like stroma or communication with the bile ducts around the tumor was found in any area of the specimen. On the basis of the World Health Organization histological classification and these pathological findings, the present case was diagnosed as invasive-type biliary cystadenocarcinoma.

Key words: biliary cystadenocarcinoma, biliary cystic tumor, intraductal papillary mucinous neoplasm, invasion, Ki-67, liver, MUC, p53

Biliary cystic tumors of the liver are rare.[1–3] According to the World Health Organization (WHO) histological classification of tumors of the liver and intrahepatic bile ducts,[3] biliary malignant cystic tumor is classified only as biliary cystadenocarcinoma (BCAC), which is defined as a usually multilocular tumor lined by mucus-secreting epithelium forming papillary folds and containing mucoid fluid but distinguished from tumors arising in a background of cystic congenital malformation, parasitic infection or hepatolithiasis. However, because the histological definition of biliary cystic tumor is not well defined, it is not useful for making a clear pathological diagnosis, especially in cases of advanced malignant biliary cystic tumor of the liver. Nakajima *et al.* classified BCAC into two subtypes: invasive and non-invasive.[4] Although several cases of invasive-type BCAC have been reported,[4–8] the detailed pathological features and pathogenesis have not yet been described, and therefore the criteria for diagnosis of biliary cystic tumor are still unclear.

Here we report a rare case of invasive biliary cystic tumor with a detailed description of the histological findings.

CLINICAL SUMMARY

A 54-year-old woman was found to have a cystic tumor in the right lobe of the liver incidentally during follow-up abdominal ultrasonography for hypertension at a local hospital, and was admitted to National Cancer Center, Tokyo, Japan. She had no symptoms. Laboratory data indicated that her serum levels of total bilirubin, alkaline phosphatase, glutamic oxaloacetic transaminase, glutamic pyruvate transaminase, CEA and AFP were all within normal limits, and only the serum level of carbohydrate antigen 19–9 was elevated (1003 U/mL). Serum markers of hepatitis A, B and C were negative. Enhanced abdominal CT showed a low-density cystic mass with wall enhancement in segment VIII of the liver. The cystic mass contained a large and prominent watery, enhancing, soft-tissue mass with calcification (Fig. 1a). No dilatation of the intrahepatic bile ducts was detected. A preoperative diagnosis of BCAC or mucin-producing cholangiocellular carcinoma (CCC) was made, and the patient underwent central

Correspondence: Hidenori Ojima, MD, Pathology Division, National Cancer Center Research Institute, 5-1-1 Tsukiji, Chuo-ku, Tokyo 104-0045, Japan. Email: hojima@ncc.go.jp

Received 9 April 2007. Accepted for publication 30 July 2007.

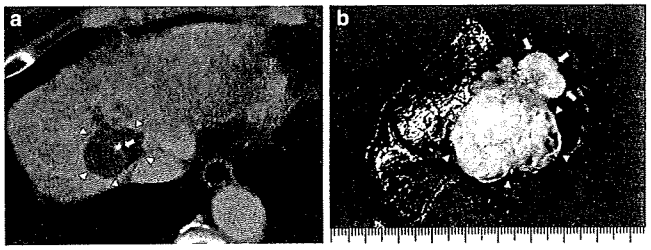

Figure 1 (**a**) Abdominal CT showing a low-density cystic mass with an enhancing wall (white arrowhead) and calcification (blue arrow) in segment VIII of the liver, but no sign of dilatation of the intrahepatic bile ducts. (**b**) Gross appearance of the tumor, showing a cystic area (white arrowhead) and a solid area (yellow arrow).

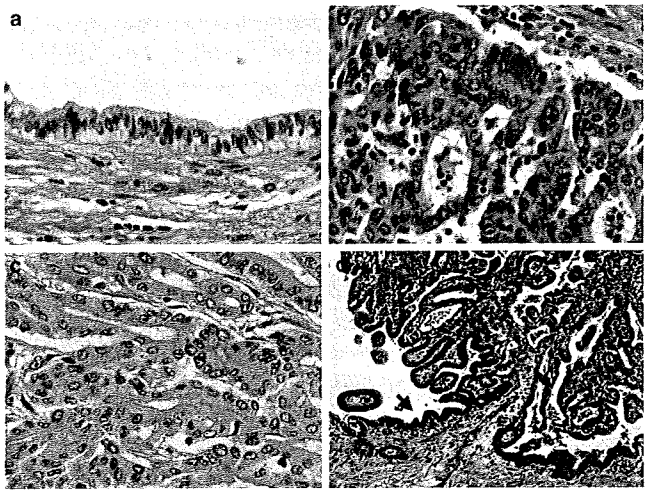

Figure 2 Microscopically, the tumor shows three types of neoplasia: (**a**) adenoma, (**b**) tubulopapillary adenocarcinoma, and (**c**) invasive adenocarcinoma. (**d**) Transitional zone between adenoma (black arrow) and tubulopapillary adenocarcinoma (*). (a–d, HE).

bisegmentectomy. At the time of writing, 21 months after surgery, the patient remained well without any evidence of tumor recurrence.

PATHOLOGICAL FINDINGS

Macroscopically the resected tumor measured 4.6 × 3.5 cm, and cystic and solid areas were seen on cut surface (Fig. 1b).

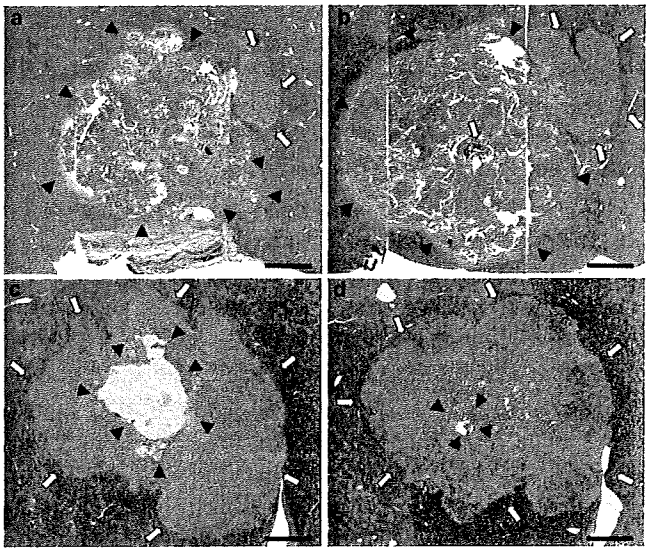

Figure 3 (**a–d**) Low-magnification view of the tumor. The cystic area (black arrowhead) and solid area (white arrow) can be identified. (**b**) Calcification (blue arrow) and overt tumor invasion through the cyst wall into the neighboring liver parenchyma are evident (HE). Bars, 5 mm.

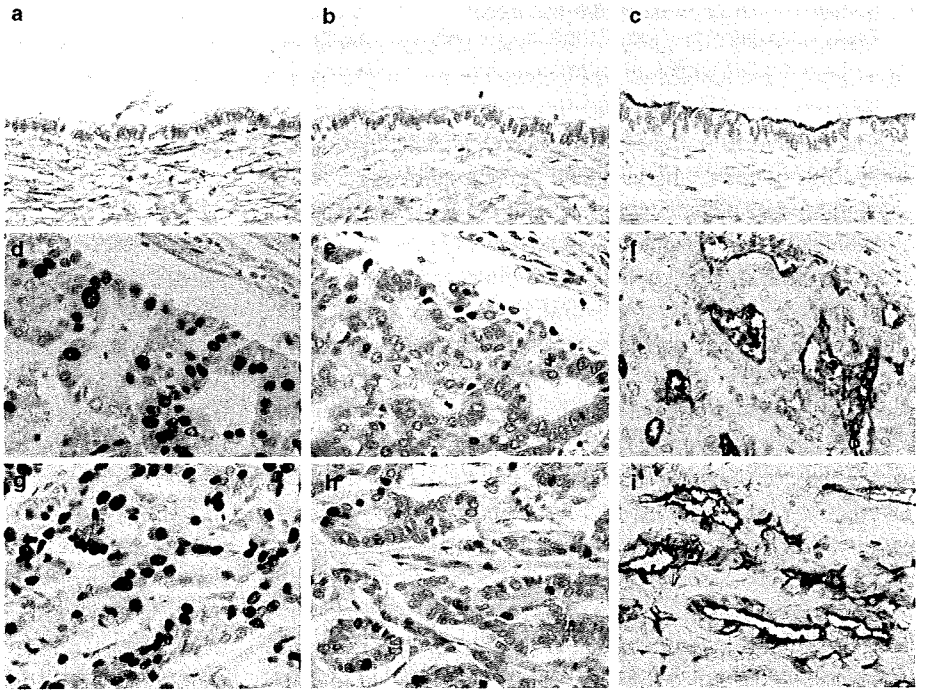

Figure 4 Immunohistochemical expression of (**a**,**d**,**g**) Ki-67 antigen, (**b**,**e**,**h**) anti-p53 protein and (**c**,**f**,**i**) MUC1 core antigen in the (**a–c**) adenoma region, (**d–f**) tubulopapillary adenocarcinoma region and (**g–i**) invasive adenocarcinoma region. The immunohistochemical expression of Ki-67 and p53 increases gradually from adenoma through to tubulopapillary adenocarcinoma, and is highest in invasive adenocarcinoma. MUC1 was positive in all three histological types.

Table 1 Immunohistochemistry

Neoplasia	% positive cells					
	MUC1	MUC2	MUC5AC	MUC6	Ki-67	p-53
Adenoma	70	–	–	–	5	2
Tubulopapillary adenocarcinoma	90	–	–	5	50	25
Invasive adenocarcinoma	100	–	–	–	70	40

–, negative (0%).

The cystic area was unilocular, lined with a smooth fibrous capsule and filled with a soft mass showing a papillary structure and thick mucin. Calcification was found in the lesion. Overt tumor invasion through the cyst wall into the neighboring liver parenchyma was also noted and connected to the solid area, which was gray–white in color.

For pathological examination the surgically resected specimen was fixed in 10% formalin for 3 days at room temperature. The entire tumor was then cut into slices at intervals of 0.7–1.0 cm, and all the tumor-containing sections were routinely processed and embedded in paraffin to examine their histological characteristics. Immunohistochemical studies were carried out on formalin-fixed, paraffin-embedded tissues. The antibodies used included those against Ki-67 antigen (clone MIB-1; Dako Cytomation, Glostrup, Denmark; dilution 1:100), p53 protein (clone DO7; Dako Cytomation; dilution 1:100), MUC1 core (clone Ma552; Novocastra Laboratories, Newcastle-upon-Tyne, UK; dilution 1:100), MUC2 (clone Ccp58; Novocastra Laboratories; dilution 1:200), MUC5AC (clone CLH2; Novocastra Laboratories; dilution 1:200), and MUC6 (clone CLH5; Novocastra Laboratories; dilution 1:100). After deparaffinization and rehydration, the sections were developed using the labeled streptavidin–biotinylated antibody technique and visualized in diaminobenzidine using conventional methods.

Microscopically the tumor had three types of neoplasia: adenoma, tubulopapillary adenocarcinoma, and invasive adenocarcinoma (Fig. 2a–c). Both adenoma and tubulopapillary adenocarcinoma corresponded to the unilocular cystic area, and invasive adenocarcinoma corresponded to the solid area. The relative area of the tumor occupied by each of these histological types was approximately 3%, 50% and 47%, respectively (Fig. 3). In the adenoma area, the cyst wall was lined with epithelial cells showing low-grade atypia, with clear eosinophilic cytoplasm and uniform, small and round nuclei (Fig. 2a). In the areas of tubulopapillary adenocarcinoma the cyst wall was covered by papillary proliferation of atypical columnar epithelial cells with eosinophilic cytoplasm and round nuclei containing multiple small nucleoli, and the tumor cells had grown into the cystic space to form a mass with a tubulopapillary structure (Figs 2b,3a,b). Calcification was seen in this area (Figs 1a,3b). The fibrous capsule had been invaded by the carcinoma cells forming the tubulopapillary mass, and invasion of the adjacent liver parenchyma was also noted (Fig. 3a–d). The areas of invasive adenocarcinoma contained tubular proliferation of atypical columnar epithelial cells with eosinophilic cytoplasm and round nuclei of various sizes (Fig. 2c), and there was evidence of portal vein and middle hepatic vein involvement. Transitional zones between adenoma and tubulopapillary adenocarcinoma (Fig. 2d), and between tubulopapillary adenocarcinoma and invasive adenocarcinoma were also found. No ovarian-like stroma was found in any area of the specimen. None of the different histological areas had any communication with the bile ducts around the tumor. The histological differential diagnosis was CCC with cyst formation or invasive adenocarcinoma derived from intraductal papillary neoplasm of the bile duct (IPN-B).

Immunohistochemistry results are summarized in Table 1. The Ki-67 labeling index was found to increase with increasing histological atypia, from 5% in the adenoma, to 50% in the tubulopapillary adenocarcinoma, and up to 70% in the invasive adenocarcinoma (Fig. 4a,d,g). The percentage of p53-positive cells also increased gradually from 2% in the adenoma to 25% in the tubulopapillary adenocarcinoma, and to 40% in the invasive adenocarcinoma (Fig. 4b,e,h). In all three types of neoplasia, MUC 1 was positive (Fig. 4c,f,i) and both MUC2 and MUC5AC were negative. MUC6 had weak focal positivity only in tubulopapillary adenocarcinoma.

On the basis of the WHO histological classification[3] and the present pathological findings, the current case was diagnosed as invasive biliary cystadenocarcinoma derived from biliary cystadenoma.

DISCUSSION

According to the WHO histological classification of tumors of the liver and intrahepatic bile ducts,[3] malignant biliary cystic tumor is classified only as BCAC. The incidence of BCAC among hepatic malignant epithelial tumors is as low as 0.41%.[1] Many studies have indicated that cystadenocarcinoma develops by malignant transformation of the epithelium of a cystadenoma.[1,9,10] Nakajima *et al.* classified BCAC into two subtypes: invasive and non-invasive.[4] In invasive-type BCAC, carcinoma extends to the liver parenchyma or adjacent organs, whereas in the non-invasive type carcinoma cell proliferation is confined to the cyst wall. On this basis, and in accordance with the WHO classification, the present case was diagnosed as invasive BCAC. Eight cases of invasive

Table 2 Reported cases of invasive-type biliary cystadenocarcinoma

Case Study no.	Age (years)	Sex	Size (cm)	No. cysts	Adenoma lesion	Transitional zone	Ovarian like (mesenchymal) stroma	Outcome
1 Iemoto *et al.*[5]	60	M	14 × 14	Multilocular	–†	+	–	Died 2 year 8 months PO
2 Nakajima *et al.*[4]	47	F	10 × 10	Unilocular	–	–	–	Died 5 months PO
3 Nakajima *et al.*[4]	43	F	9 × 6	Unilocular	–	–	–	Died 1 year PO
4 Nakajima *et al.*[4]	65	F	14 × 14	Multilocular	–†	+	–	Died 10 months PO
5 Stacher *et al.*[6]	77	F	11 × 10 × 14	Multilocular	–	–	ND	Well 8 months PO
6 Bardin *et al.*[7]	43	F	18 × 13.5 × 8	Multilocular	–	–	–	ND
7 Murakami *et al.*[8]	82	F	10 × 10 × 9.5	Multilocular	–	–	–	Died 1 year PO
8 Present study	54	F	4.6 × 3.5	Unilocular	+	+	–	Well 1 year 9 months PO

†Focal benign-appearing epithelium.
+, present; –, absent; ND, not described; PO, postoperatively.

BCAC have been reported in the English-language literature (Table 2). All but one of the patients were women, and their ages ranged from 43 to 82 years (mean, 58.9 years). Multilocular lesions were evident in five cases, and unilocular lesions in two. The tumors ranged in size from 4.6 to 18 cm (mean 11.7 cm). However, these patients had no clear and distinctive clinicopathological characteristics (e.g. age, outcome, tumor size etc.), and because no detailed study of invasive biliary cystic tumor has yet been done, the clinicopathological features remain largely unknown.

Recently Zen *et al.* reported that biliary cystic tumor with bile duct communication and without ovarian-like stroma might be a cystic variant of IPN-B rather than a true biliary cystic neoplasm.[11] Several studies have indicated that IPN-B is the counterpart of intraductal papillary mucinous neoplasm of the pancreas (IPMN-P),[12–14] and that the immunophenotypes of IPN-B resemble those of IPMN-P.[15,16] If the term 'biliary cystadenoma' or 'cystadenocarcinoma' is restricted to true cystic neoplasms with an ovarian-like stroma, as in the pancreas, previously reported biliary cystic tumors with an ovarian-like stroma have occurred only in female patients.[17,18] From this viewpoint, the present case was morphologically similar to invasive adenocarcinoma derived from IPN-B, even though bile duct communication was not evident. The present case was of the pancreatobiliary type according to the IPMN-P classification.[19–22] However, the immunohistochemical expression pattern observed was not typical of IPN-B. Most IPN-B have high expression of MUC2 and MUC5AC, but the present case was negative for both.

We consider that in some cases of BCAC, the ovarian-like stroma may disappear during the process of malignant transformation from biliary cystadenoma. Devaney *et al.* reported that non-specific reactive changes were evident in the cyst wall (typically between the ovarian-like zone and the fibrous pseudocapsule),[17] and that ovarian-like stroma was abundant in some cases but focal in others. Similar findings were obtained in other cases we have examined (data not shown). Moreover, most patients with biliary cystadenoma have symptoms of abdominal discomfort and the tumor is large at the time of discovery (mean diameter 15–16 cm).[17,18] These facts suggest that microrupture of the cyst and reactive changes in the cyst wall may occur repeatedly during growth of the tumor, and that symptoms do not become evident until the tumor becomes large. Therefore, the area of ovarian-like stroma may vary. If such events do, in fact, occur, some cases of BCAC derived from cystadenoma may not have an ovarian-like stroma. We consider that the present case may represent this type of BCAC.

On the other hand, the present tumor had invasive solid areas that resembled CCC. Furthermore, there was a cystic component and invasive area lined with epithelial cells showing low-grade atypia that did not communicate with the intrahepatic bile ducts. Features often seen in CCC are dilatation of the intrahepatic bile ducts surrounding the tumor and *in situ* carcinoma in the bile duct epithelium, which are evidence for the theory that CCC arises in the bile duct epithelium. However, we did not detect any such features, and on the basis of the pathological evidence we concluded that the tumor was not CCC.

One of the most interesting features of the present case was that discrete areas of adenoma, tubulopapillary adenocarcinoma and invasive adenocarcinoma were clearly evident within the same specimen. Moreover, transitional zones were also evident between adenoma and tubulopapillary adenocarcinoma, and between tubulopapillary adenocarcinoma and invasive adenocarcinoma. To our knowledge this combination of pathological features has never been reported previously, and we consider that they indicate the sequence underlying the development of invasive biliary cystic tumor. In addition, we found that the immunohistochemical expression of Ki-67 and p53 increased gradually from adenoma lesion through to tubulopapillary adenocarcinoma, and was highest in invasive adenocarcinoma, indicating that the degree of malignancy progressed with increasing histological atypia, from adenoma to invasive adenocarcinoma.[23,24] It was also interesting that high immunohistochemical expression of MUC1 was observed even in adenoma, which shows low histological atypia. MUC1 expression is usually high in invasive-type

intrahepatic bile duct tumors that have a poor prognosis.[25] It is considered that this type of invasive biliary cystic tumor may have a malignant character resembling CCC from as early as the adenoma stage,[26,27] suggesting that the pathogenesis involves the adenoma–cystadenocarcinoma–invasive adenocarcinoma sequence.

In conclusion, we have presented a rare case of invasive biliary cystic tumor without an ovarian-like stroma and have characterized the apparent sequence underlying its malignant transformation, on the basis of detailed histological examination. We believe that the features of the present case are important when considering the pathogenesis or diagnostic criteria of advanced-type biliary cystic tumor.

REFERENCES

1 Takayasu K, Muramatsu Y, Moriyama M *et al.* Imaging diagnosis of bile duct cystadenocarcinoma. *Cancer* 1988; **61**: 941–6.
2 Ishak KG, Willis GW, Cummins SD *et al.* Biliary cystadenoma and cystadenocarcinoma: Report of 14 cases and review of the literature. *Cancer* 1977; **39**: 322–38.
3 Wittekind C, Fischer HP, Ponchon T. Bile duct cystadenoma and cystadenocarcinoma. In: Hamilton, SR, Aaltonen LA, eds. *WHO Classification. Tumor of the Digestive System.* Lyon: IARC Press, 2000;182–3.
4 Nakajima T, Sugano I, Matuzaki O *et al.* Biliary cystadenocarcinoma of liver. A clinicopathologic and histochemical evaluation of nine cases. *Cancer* 1992; **69**: 2426–32.
5 Iemoto Y, Kondo Y, Nakakno T, Tsuchiya K, Ohto M. Biliary cystadenocarcinoma diagnosed by liver biopsy performed under ultrasonographic guidance. *Gastroenterology*, 1983; **84**: 399–403.
6 Stacher R, Szolar DH, Bacher H, Preidler KW. Mucinous biliary cystadenocarcinoma containing gas bubbles secondary to duodenal invasion. *Br J Radiology* 1998; **71**: 683–5.
7 Bardin RL, Trupiano JK, Howerton RM, Geisinger KR. Oncocytic biliary cystadenocarcinoma: A case report and review of the literature. *Arch Pathol Lab Med* 2004; **128**: e25–8.
8 Murakami Y, Kanehiro T, Yokoyama Y *et al.* Successful complete resection of biliary cystadenocarcinoma after percutaneous transhepatic portal embolization. *Surgery*, 2005; **137**: 577–9.
9 Kubota E, Katsumi K, Iida M *et al.* Biliary cystadenocarcinoma followed up as benign cystadenoma for 10 years. *Gastroenterology* 2003; **38**: 278–82.
10 Ishak KG, Goodman ZD, Stocker JT. *Tumors of the Liver and Intrahepatic Bile Ducts. Atlas of Tumor Pathology. Third Series, Fascicle 31.* Washington, DC: Aimed Forces Institute of Pathology, 1999.
11 Zen Y, Fujii T, Itatsu K *et al.* Biliary cystic tumors with bile duct communication: A cystic variant of intraductal papillary neoplasm of the bile duct. *Mod Pathol* 2006; **19**: 1243–54.
12 Abraham SC, Lee JH, Boitnott JK, Argani P, Furth EE, Wu TT. Microsatellite instability in intraductal papillary neoplasms of the biliary tract. *Mod Pathol* 2002; **15**: 1309–17.
13 Abraham SC, Lee JH, Hruban RH *et al.* Molecular and immunohistochemical analysis of intraductal papillary neoplasms of the biliary tract. *Hum Pathol* 2003; **34**: 902–10.
14 Zen Y, Sasaki M, Fujii T *et al.* Different expression patterns of mucin core proteins and cytokeratins during intrahepatic cholangiocarcinogenesis from biliary intraepithelial neoplasia and intraductal papillary neoplasm of the bile duct: An immunohistochemical study of 110 cases of hepatolithiasis. *J Hepatol*, 2006; **44**: 350–58.
15 Chen TC, Nakanuma Y, Zen Y *et al.* Intraductal papillary neoplasia of the liver associated with hepatolithiasis. *Hepatology*, 2001; **34**: 651–8.
16 Shibahara H, Tamada S, Goto M *et al.* Pathologic features of mucin-producing bile duct tumors: Two histopathologic categories as counterparts of pancreatic intraductal papillary-mucinous neoplasms. *Am J Surg Pathol* 2004; **28**: 327–38.
17 Devaney K, Goodman ZD, Ishak KG. Hepatobiliary cystadenoma and cystadenoma. *Am J Surg Pathol* 1994; **18**: 1078–91.
18 Wheeler DA, Edmondson HA. Cystadenoma with mesenchymal stroma (CMS) in the liver and bile ducts. A clinicopathologic study of 17 cases, 4 with malignant change. *Cancer* 1985; **56**: 1434–45.
19 Adsay NV, Conlon KC, Zee SY, Brennan MF, Klimstra DS. Intraductal papillary-mucinous neoplasms of the pancreas: An analysis of in situ and invasive carcinomas in 28 patients. *Cancer* 2002; **94**: 62–77.
20 Luttges J, Zamboni G, Longnecker D, Kloppel G. The immunohistochemical mucin expression pattern distinguishes different types of intraductal papillary mucinous neoplasms of the pancreas and determines their relationship to mucinous noncystic carcinoma and ductal adenocarcinoma. *Am J Surg Pathol* 2001; **25**: 942–8.
21 Yonezawa S, Nakamura A, Horinouchi M, Sato E. The expression of several types of mucin is related to the biological behavior of pancreatic neoplasms. *J Hepatobiliary Pancreat Surg* 2002; **9**: 328–41.
22 Furukawa T, Kloppel G, Volkan Adsay N *et al.* Classification of types of intraductal papillary-mucinous neoplasm of the pancreas: A consensus study. *Virchows Arch* 2005; **447**: 794–9.
23 Murakami M, Sasaki T, Kuwada Y, Yamasaki S, Kuwahara K, Chayama K. Prognostic value of p53 and Ki-67 expression in resected or biopsy specimens of bile duct carcinoma. *Oncol Rep* 2003; **10**: 1091–6.
24 Jackson PA, Green MA, Pouli A, Hubbard R, Marks CG, Cook MG. Relation between stage, grade, proliferation, and expression of p53 and CD44 in adenomas and carcinomas of the colorectum. *J Clin Pathol* 1995; **48**: 1098–101.
25 Higashi M, Yonezawa S, Ho JJ *et al.* Expression of MUC1 and MUC2 mucin antigens in intrahepatic bile duct tumors: Its relationship with a new morphological classification of cholangiocarcinoma. *Hepatology* 1999; **30**: 1347–55.
26 Amaya S, Sasaki M, Watanabe Y *et al.* Expression of MUC1 and MUC2 and carbohydrate antigen Tn change during malignant transformation of biliary papillomatosis. *Histopathology* 2001; **38**: 550–60.
27 Sasaki M, Nakanuma Y. Expression of mucin core protein of mammary type in primary liver cancer. *Hepatology* 1994; **20**: 1192–7.

Journal of Surgical Oncology 2007;96:160–165

Clinical Impact of the Surgical Margin Status in Hepatectomy for Solitary Mass-Forming Type Intrahepatic Cholangiocarcinoma Without Lymph Node Metastases

KAZUAKI SHIMADA,[1]* TSUYOSHI SANO,[3] YOSHIHIRO SAKAMOTO,[1] MINORU ESAKI,[1] TOMOO KOSUGE,[1] AND HIDENORI OJIMA[2]

[1]*Department of Hepatobiliary and Pancreatic Surgery Division, National Cancer Center Hospital, Japan*
[2]*Pathology Division, National Cancer Center Research Institute, Tokyo, Japan*
[3]*Department of Gastroenterological Surgery, Aichi Cancer Center, Nagoya, Japan*

Background and Objectives: The clinical impact of the surgical margin status in macroscopic curative hepatectomy for intrahepatic cholangiocarcinoma (ICC) has not yet been fully investigated.

Methods: The data of 57 consecutive patients with mass-forming (MF) type ICC who underwent macroscopic curative hepatectomy during a 10-year period were retrospectively examined, and the relationship between the surgical margin status and patient survival was analyzed.

Results: Lymph node metastases were found to be independently associated with poor survival. The overall 5-year survival rates and the median survival term in the 38 patients without lymph node metastases were 56.8% and 62 months, respectively. Among these 38 patients, the survival rate was better in the negative surgical margin group as compared with that in the positive surgical margin group. However, there was no statistically significant difference between the narrow and wide surgical margin groups.

Conclusions: Negative surgical margin had a definite favorable impact on the survival of patients with a solitary ICC without lymph node metastases. Surgery should be conducted in patients without lymph node metastases even if a wide surgical margin cannot be obtained, but careful attention should be paid not to expose tumors during hepatic dissection.

J. Surg. Oncol. 2007;96:160–165. © 2007 Wiley-Liss, Inc.

KEY WORDS: **mass-forming type; intrahepatic cholangiocarcinoma; hepatectomy; curative resection; surgical margin**

INTRODUCTION

Intrahepatic cholangiocarcinoma (ICC) has been considered a rare primary hepatic tumor. Recently, however, the incidence and mortality of ICC have increased [1]. ICCs have been classified into several types based on the macroscopic appearance of the tumors [2–4]. Mass-forming (MF) type ICC, which is the most commonly encountered type in the clinical setting, is a round, potato-shaped lesion with a distinct border in the liver parenchyma, and is sometimes difficult to differentiate from hepatocellular carcinoma and metastatic tumors from other organs [5]. The optimal extent of hepatectomy and the appropriate width of the surgical margin for other hepatic malignancies have been evaluated to improve the surgical outcomes, but the clinical significance of the surgical margin status in

*Correspondence to: Kazuaki Shimada, Department of Hepatobiliary and Pancreatic Surgery Division, National Cancer Center Central Hospital; 5-1-1 Tsukiji; Chuo-ku, Tokyo 104-0045, Japan. Fax: 81 3 3542 3815. E-mail: kshimada@ncc.go.jp

Received 28 September 2006; Accepted 22 January 2007
DOI 10.1002/jso.20792
Published online 18 April 2007 in Wiley InterScience (www.interscience.wiley.com).

hepatectomy with MF type ICC has not been fully investigated [6–11].

Curative resection remains one of the most important prognostic factors in patients with ICC [12–14]. However, it is often difficult to obtain a generous surgical margin in cases of ICC because the majority of patients present with large, often centrally located tumors. The most frequent mode of spread into the liver is direct invasion into the adjacent liver parenchyma through the sinusoids [15]. The clinical importance of an adequate surgical margin to ensure removal of the micrometastases in the surrounding liver parenchyma still remains unclear.

In the present study, data of a relatively large number of patients with typical MF type ICC who underwent hepatectomy at one Japanese institution were examined to identify the prognostic factors for survival, with special reference to the status of the surgical margin.

PATIENTS AND METHODS

Between January 1, 1995 and December 31, 2004, 111 patients with ICC underwent macroscopic curative hepatectomy, at the National Cancer Center Hospital, Tokyo, Japan. ICC was defined as the carcinoma arising from second-order or more distal branches of the intrahepatic bile ducts; hilar bile duct cholangiocarcinoma and gallbladder cancer were excluded. The criteria for resectability were absence of peritoneal dissemination, bulky lymph node metastasis, paraaortic lymph node metastasis, and/or intrahepatic metastasis in the remnant liver. Macroscopic curative resection was defined as the absence of apparent tumor residue in the operative field. Based on the macroscopic classification proposed by the Liver Cancer Study Group of Japan, the resected tumors were classified into the MF type (n = 58, 52%), the periductal infiltrating (PI) type (n = 9, 8%), the intraductal growth (IG) type (n = 6, 5%), the MF plus PI type (n = 32, 29%), and the MF plus IG type (n = 6, 5%) [3]. Fifty-eight patients with MF type ICC were enrolled in the present study. There were 33 men and 25 women ranging in age from 44 to 84 years (mean, 65 years).

The extent of hepatic resection was dependent on tumor size and location. The distribution of the types of hepatectomy was: partial resection (n = 6, 10%), segmentectomy (n = 6, 10%), left lobectomy (n = 15, 26%), right lobectomy (n = 21, 36%), right trisegmentectomy (n = 2, 4%), left trisegmentectomy (n = 6, 10%), and central bisegmentectomy (n = 2, 4%). In 31 patients (53%) suspected to have lymph node involvement based on preoperative imaging or intraoperative findings, lymph node dissection was performed around the hepatoduodenal ligament, posterior to the upper portion of the pancreatic head, and along the common hepatic artery. Resection of the biliary confluence and extrahepatic bile duct, portal vein, and hepatic artery, and combined resection of the inferior vena cava was performed on 13 (22%), 3 (5%), 1 (2%), and 6 patients (10%), respectively. Among the 58 patients, there were no operative or in-hospital deaths. The patients were closely followed up every 3 months at an outpatient clinic with measurement of the serum levels of carbohydrate antigen 19-9 (CA19-9) and carcinoembryonic antigen (CEA), chest x-ray, and ultrasonography or computed tomography. The specific sites of first disease recurrence were analyzed. Radiologic evidence of tumor recurrence was considered acceptable even in the absence of biopsy confirmation. When progression of the disease was confirmed by repeated imaging studies, the date of the first suspicious radiologic finding was considered as the date of initial disease recurrence. One patient was lost to follow-up and was excluded from the follow-up analysis. The median follow-up duration of the remaining 57 patients was 19 months (range, 2–115 months).

In these 57 patients, the significance of 14 clinicopathological factors potentially influencing the prognosis was analyzed using the log-rank test. The continuous variables were classified into two groups according to the median value of each factor. Multivariate regression analysis was performed using the Cox proportional hazards model and associations with $P < 0.10$ were entered into the final model adopted. The surgical margin was divided into the following three categories: a wide surgical margin group with a negative surgical margin historically measured as >5 mm in width; a narrow surgical margin group with a negative surgical margin historically measured as ≤5 mm in width; and a positive surgical margin group with a surgical margin involved with cancer cells around non-encapsulated tumors, which was confirmed by microscopic examination. The relationship between the surgical margin status and 10 possible prognostic factors was examined. Trends and differences were tested by the Yates' chi-square test. Survival estimates were calculated by the Kaplan–Meier method and compared using the log-rank test. All statistical analyses were performed using the Software Package for the Social Sciences 11.5J for Windows® (SPSS, Chicago, Illinois). A two sided $P < 0.05$ was considered as denoting significance.

RESULTS

The overall 1- and 5-year survival rates were 73.3% and 43.7%, respectively, in 57 patients with MF type ICC. The mean survival time was compared among the possible predictors (Table I). Lymph node involvement and intrahepatic metastasis were determined to be significantly unfavorable prognostic factors by univariate

TABLE I. Possible Clinical and Pathological Risk Factors for Survival in Patients With MF

Factors		No. of patients	5-year survival rate (%)	Median survival term (months)	*P*-value
Overall		57 (100)	43.7	31	—
Age (median; 65 years)	≤65	30 (53)	45.5	25	0.8653
	>65	27 (47)	41.1	31	
Gender	M	32 (56)	54.4	62	0.5439
	F	25 (44)	35.2	26	
Symptoms	Absent	43 (82)	42.5	31	0.5056
	Present	14 (18)	18.2	26	
Ca19-9 (median: 126 U/ml)	≤126	27 (52)	48.7	30	0.5753
	>126	25 (48)	36.3	31	
CEA (median: 3.0 ng/ml)	≤3.0	35 (61)	48.7	30	0.4893
	>3.0	22 (39)	34.5	31	
Size (median: 5.2 cm)	≤5.2	29 (51)	47.3	30	0.3589
	>5.2	28 (49)	39.1	31	
Intrahepatic metastases	Absent	36 (68)	54.4	62	0.0124
	Present	21 (32)	23.7	14	
Portal vein invasion	Absent	19 (33)	44.6	31	0.6651
	Present	38 (67)	45.5	32	
Hepatic vein invasion	Absent	33 (58)	49.1	32	0.3672
	Present	24 (42)	35.1	22	
Bile duct invasion	Absent	21 (37)	61.3	–	0.2173
	Present	36 (63)	39.5	25	
Histological differentiation	Well	13 (23)	60.6	–	0.1365
	Mod/poor	44 (77)	36.0	26	
Lymph node metastases	Negative	38 (67)	56.8	62	0.0054
	Positive	19 (33)	18.7	17	
Extent of hepatectomy	Segmentectomy and less	12 (21)	12.6	26	0.1578
	Lobectomy and more	45 (79)	53.6	62	
Surgical margin	Negative	44 (77)	56.8	62	0.0621
	Positive	13 (23)	16.7	20	

analysis. Patients with a negative surgical margin tended to have a better survival rate than those with a positive surgical margin. However, the difference was not statistically significant ($P = 0.0621$). When the significant prognostic factors as determined by univariate analysis were assessed by multivariate analysis, only lymph node metastasis was found to be independently associated with poor survival, with a hazard ratio (95% confidence interval) of 2.934 (1.329–6.475: $P = 0.008$).

Figure 1 shows the result of survival analysis in the 57 patients with/without lymph node metastasis and with/without intrahepatic metastasis. The overall 1- and 5-year survival rates in the 26 patients with neither lymph node nor intrahepatic metastasis were 96.1% and 65.3%, respectively. In contrast, nine patients with both lymph node metastasis and intrahepatic metastasis survived for no longer than 25 months, with a median survival time of 17 months.

Figure 2 shows a comparison of the cumulative survival rates by the surgical margin status in the 38 patients with no lymph node metastasis. Compared with the negative (wide and narrow) surgical margin group, survival was significantly poorer in the positive

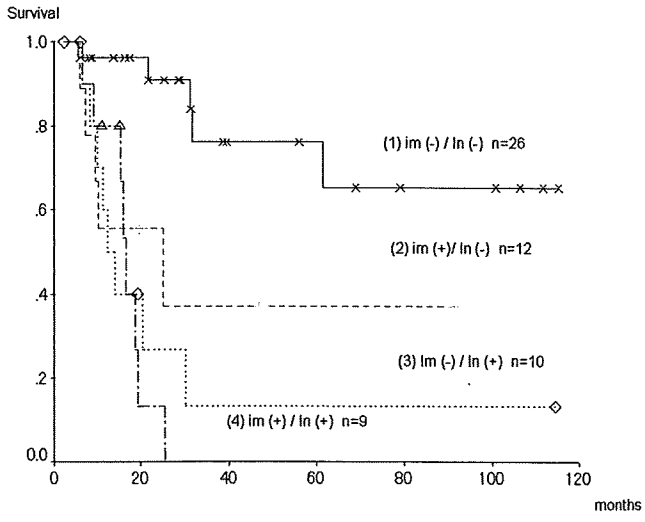

Fig. 1. Overall patient survival rate according to the presence of lymph node metastasis and/or intrahepatic metastasis. ln: lymph node metastasis, im: intrahepatic metastasis. The statistically significant differences revealed were: (1) versus (2), $P = 0.0001$; (1) versus (3), $P < 0.0001$; (1) versus (4), $P = 0.0135$.